Journal of Hydrology: Regional Studies 26 (2019) 100636

Contents lists available at ScienceDirect

Journal of Hydrology: Regional Studies

journal homepage: www.elsevier.com/locate/ejrh

Hydrogeochemical and mineralogical factors influencing uranium in background area groundwater wells: Grants, New Mexico

Shannon Ulrich[a,*], Jeffrey Gillow[b], Shawn Roberts[c], Gregory Byer[d], Julie Sueker[a], Kathryn Farris[e]

[a] Arcadis North America, 11001 West 120th Avenue, Suite 200, Broomfield CO, 80021, United States
[b] Jacobs Engineering Group, 9191 South Jamaica Street, Englewood, CO 80112, United States
[c] Arcadis North America, 735 Tank Farm Road, Suite 150, San Luis Obispo, CA 93401, United States
[d] Arcadis North America, 150 West Market Street, Suite 728, Indianapolis IN 46204, United States
[e] Arcadis North America, 855 Route 146 Suite 210, Clifton Park NY 12065, United States

ARTICLE INFO

Keywords:
Grants mineral belt
San Mateo Creek Basin
Eroded sandstone bedrock
Alluvial aquifer
Uranium
Lithologic analysis

ABSTRACT

Study region: Lower San Mateo Creek Basin (SMCB), New Mexico
Study focus: Groundwater in the alluvial aquifer of the lower SMCB has a high concentration of total dissolved solids, alkalinity, and dissolved uranium at concentrations above USEPA limits; the source of the water quality was investigated through evaluation of geology, mineralogy, and geochemistry of sediments and groundwater. Surface-expressing bedrock in the larger Basin is dominated by uranium-bearing units such as the Morrison Formation and Dakota Sandstone; erosion of these units contributed sediment to Quaternary alluvium valley fill in the Basin with heterogeneous distribution of uranium. The potential for uranium-bearing alluvial fill to affect the groundwater quality was investigated upgradient of the Grants Reclamation Project (GRP), a former uranium milling facility in the lower SMCB, by hydrogeochemical and geophysical methods.
New hydrological insights for the region: Uranium is primarily associated with fine-grained materials (clay/silt) and is labile depending upon sediment geochemical conditions. Natural occurrence of uranium minerals in SMCB alluvial sediments here results in concentrations in groundwater greater than the USEPA water quality standards; as such, site-specific standards are established and supported by the findings of this work. Regional groundwater systems, derived from weathered mineralized bedrock, require careful evaluation of water quality to understand background conditions; uranium in groundwater results from hydrogeochemical processes at the interface of fine and coarse grained sediments within the aquifer.

1. Introduction

The Cretaceous and Jurassic sandstone-hosted uranium deposits of the Grants-Ambrosia Lake uranium district in New Mexico were the sites of numerous uranium mines and associated milling facilities. Quaternary deposits adjacent to these uranium-bearing bedrock units host an alluvial groundwater system of varying water quality and quantity. The relationship between the mineralogy of the Quaternary deposits and groundwater quality was investigated near the GRP site, a former uranium mill (the Homestake Mill) in the center of the lower San Mateo Creek Basin (hereafter referred to as the lower Basin; Fig. 1). The Homestake Mill operated from

* Corresponding author.
E-mail address: Shannon.Ulrich@arcadis.com (S. Ulrich).

https://doi.org/10.1016/j.ejrh.2019.100636
Received 18 May 2019; Received in revised form 15 October 2019; Accepted 16 October 2019

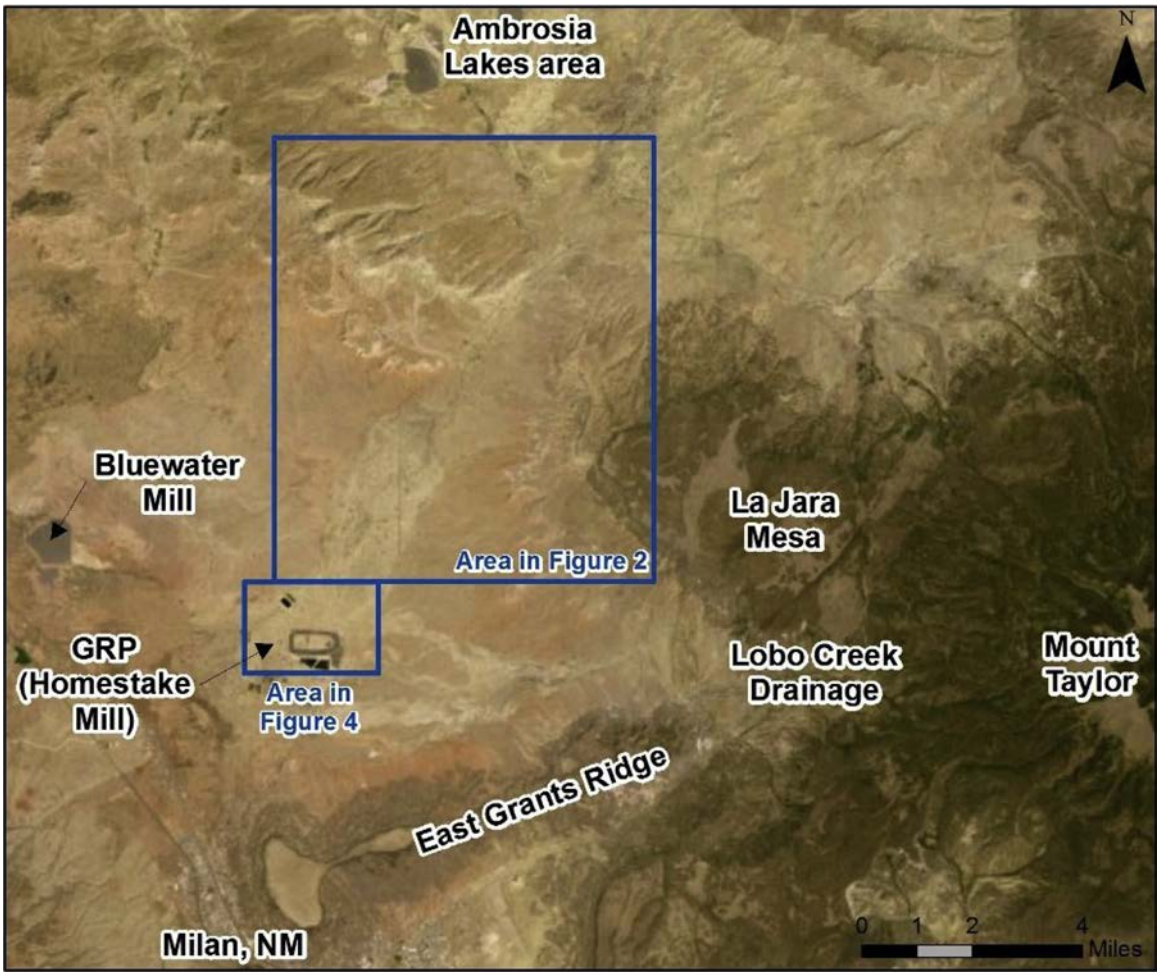

Fig. 1. Regional map of the lower Basin.

1958 to 1990 under a license from the Nuclear Regulatory Commission (NRC), and since 1977, active groundwater remediation was initiated to address constituents released from a tailing impoundment; investigation work throughout this time has primarily focused on delineating the areas of the alluvial aquifer affected by milling. The study presented here was designed to define processes that dictate water quality, identify sources of constituents to groundwater, and establish the technical basis for groundwater restoration at the former uranium mill. The United States Environmental Protection Agency (USEPA) initiated a field investigation in 2016 to further evaluate groundwater quality upgradient of the mill (Harte et al., 2019; Blake et al., 2017). The study builds upon the work completed by the USEPA and their collaborators at the United States Geological Survey (USGS).

1.1. Uranium, selenium, molybdenum, and vanadium geochemistry in roll-front deposits

During the formation of continental crust, uranium, selenium, molybdenum, and vanadium undergo a series of fractionation events resulting in highly variable concentrations in different rock types. Uranium exhibits dynamic chemical behavior, readily transforming between dissolved and solid forms, leading to significant migration and redistribution in geologic systems. Uranium can be leached from host mineral phases to surface water and/or groundwater through a variety of processes, but most commonly through exposure to carbonate-rich waters generated through carbonate mineral dissolution (Langmuir, 1978). Redeposition of uranium occurs in sandstones and other porous host materials in association with geochemically reducing groundwaters or reduced materials. The precipitation of uranium at this redox front forms what is referred to as a “roll-front” deposit. Pyrite and organic matter are integral parts of sandstone strata-bound uranium ore and roll-front deposits such as in the Grants Mineral Belt, providing the reducing power to precipitate uraninite (UO_2) in the sandstone host (Brookins, 1982; Granger and Warren, 1974; Spirakis, 1996; Plant et al., 1999). At the redox interface, mackinawite (FeS), pyrite (FeS_2), siderite ($FeCO_3$), iron oxyhydroxide minerals, and elemental selenium (Se^0) are frequently encountered (Granger and Warren, 1974). Within the Basin, the sequence of this mineralization is understood to be selenium first or with pyrite, uranium and vanadium concurrently, and molybdenum last (Brookins, 1982), frequently concurrently with the reduction and precipitation of clay or clay-like minerals (Brookins, 1990).

Other trace metals/metalloids are nonuniformly distributed through the Grants Mineral Belt. Reduced-phase selenium is present in both ore-bearing and barren sandstone as ferroselite within the Poison Canyon unit in the Brushy Basin Member of the Morrison Fm. (Cannon, 1953). Uranium selenites, seleniferous pyrite, and elemental selenium (Brookins, 1982) have been shown to be present in high concentrations in these redox-interface environments (Finch and Murakami, 1999). Molybdenum is commonly present in roll-front deposits as jordisite (MoS_2) and as reduced molybdenum (Mo[IV]) in pyrite (Brookins, 1982). Uranium molybdates are also present in ore-grade material, with molybdenum present as Mo(VI) and uranium of mixed valence as U(IV) and U(VI). Mixed-valence uranium molybdates form primarily where uraninite and molybdenum-bearing minerals are undergoing weathering and oxidation (Finch and Murakami, 1999). Vanadium has been shown to occur in clays in the Grants Mineral Belt as reduced V(IV) or V(III) and is frequently associated with uranium ore. Only by severe alteration can vanadium be released (as oxidized V[V]) from the clay mineral structure (Brookins, 1982). Ambrosia Lake uranium ore can contain up to 3.2% vanadium oxide (Lee, 1976) and vanadium is considered a pathfinder element for uranium ore in this region (Brookins, 1982). Uranyl vanadates are important uranium ores in the Colorado Plateau and form where reduced uranium minerals (e.g., uraninite) and reduced vanadium minerals (e.g., montroseite) undergo oxidation; the resultant minerals such as carnotite $[K_2(UO_2)_2(V_2O_8)(H_2O)_3]$ are very stable (Finch and Murakami, 1999). The weathering of uranium-bearing vanadates, molybdates, and selenates in alluvial sediments can result in the release of these elements into the groundwater system. Alkalinity plays a large role in the dissolution and persistence of uranium in groundwater systems.

1.2. Regional natural sources of U, Se, and V

Of the numerous uranium-bearing geologic units present in the Grants-Ambrosia Lake uranium district, several of important economic interest crop out in the Basin, notably as weathered bluffs surrounding the lower Basin (Fig. 2). The majority of the

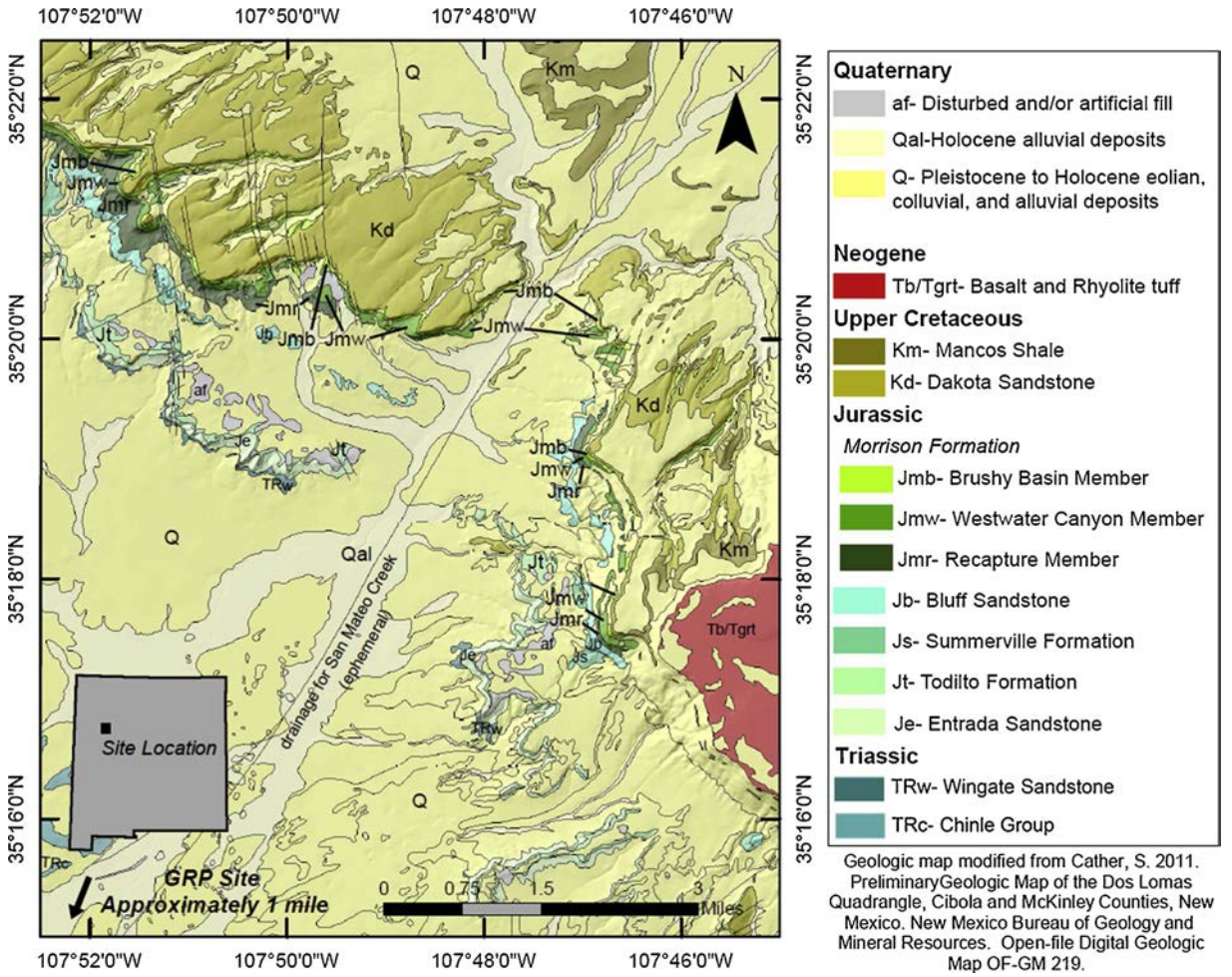

Fig. 2. Geologic map of part of the upper San Mateo Creek Basin (north), transitioning to the lower San Mateo Creek Basin (south). The Jurassic Morrison Formation units crop out along the bluff faces running northwest to southeast.

uranium-bearing units in the region occur in north-northeast dipping Jurassic and Cretaceous units, including the Jurassic Todilto Limestone, Morrison Fm. Recapture, Westwater Canyon, and Brushy Basin Members, and the Cretaceous Dakota Sandstone and Mancos Shale. The primary uranium deposits in the Morrison Fm. were formed through deposition at a groundwater geochemical interface with no consensus on the exact origin, although deposition with humates and other organic material or deposition at a brine-groundwater interface are common origin theories (McLemore, 2010). After formation of the primary sandstone uranium deposits, oxidizing groundwaters remobilized some of the primary deposits and redistributed uranium at a redox interface (roll-front deposit). Where oxidized waters could not access, remnant-primary sandstone uranium deposits remained (McLemore, 2010). Penecontemporaneously formed uranium-vanadium assemblages are abundant in the deposits (Brookins, 1982; McLemore, 2010). In addition, uranium is complexed and sorbed onto clay minerals within the mineral belt (Brookins, 1979). Uranium deposition and resultant concentrations in the sandstones are highly variable. The Morrison Fm. crops out approximately 5 miles to the north and hydrogeologically upgradient of the site investigated in this work; weathering of these units over geologic time (estimated as hundreds of years for the shallowest alluvial sediments to thousands or tens of thousands of years for the deeper sediments (Leopold and Snyder, 1951)), along with weathering of the Dakota Sandstone, has deposited sediments in the alluvial basin upgradient and throughout the site (McLemore, 2010).

Unoxidized mineral assemblages in the Grants Mineral Belt include smectites, illites, and authigenic chlorites in association with pyrite- and organic-rich, calcite-cemented sandstones (Granger, 1963). The authigenic chlorites are often vanadiferous and form alongside coffinite and uraninite (Brookins, 1982), indicating that uranium's association with vanadium and authigenic clays is due to co-genesis. Oxidized mineral assemblages are characterized by kaolinite with detrital chlorite and re-worked smectites that co-occur with ferric oxyhydroxide-bearing, organic carbon-free, sulfate-carbonate-cemented sandstone (Brookins, 1990).

In the Grants region, the Todilto Limestone consists of thin- to thick- bedded limestone with basal, platy deposits of uranium (Heinrich, 1958) associated with fractures containing geochemically reducing organic matter (McLemore, 2010). Uranium is primarily present in the form of uraninite or less commonly as uraniferous fluorite (Heinrich, 1958) but is rare to absent in/near the Todilto Limestone gypsum-anhydrite beds (Lovering, 1956; Hilpert, 1969). Other mineral components of the Todilto Limestone include pyrite, barite, calcite, and fluorite with secondary uranium-vanadium minerals carnotite and tyuyamunite (Heinrich, 1958).

The Recapture Member of the Morrison Fm. consists of alternating fluvially deposited mudstones and sandstones (Freeman and Hilpert, 1956; Thaden et al., 1967; Santos, 1970) with lenses of Westwater Canyon Member sandstone in upper sections (Cather, 2011). The Recapture Member in the lower Basin has not been shown to contain the same levels of uranium and vanadium minerals as other reaches of the unit (McLemore, 2007) but does consistently contain significant selenium (Beath et al., 1940).

The Westwater Canyon Member of the Morrison Fm. consists of fluvially deposited arkosic sandstones with angular grains of unaltered feldspar (Freeman and Hilpert, 1956; Santos, 1970; Pierson and Green, 1977) with clay cement (Heinrich, 1958), and interbedded mudstones (Freeman and Hilpert, 1956; Santos, 1970; Pierson and Green, 1977). Asphaltite and calcite have replaced clay cement between sand grains and the organic-rich asphaltite served as a precipitant for uranium (Heinrich, 1958). The ore is predominantly coffinite dispersed in pyrite and asphaltite and in some places contains uranium-vanadium mineral tyuyamunite (Meunier, 1994). Clays are primarily montmorillonite and kaolinite (Freeman and Hilpert, 1956; Santos, 1970) with some illite (Brookins, 1990). Due to its consistently high uranium content, the Westwater Canyon Member is one of the most mined units in the region (McLemore, 2010). The high potassium feldspar content in this unit is an identifying characteristic, distinguishing the Westwater Canyon and Brushy Basin Members from other geologic units in the region (Freeman and Hilpert, 1956).

The Brushy Basin Member of the Morrison Fm. consists of fluvially deposited claystone with some interbedded and otherwise massive semi-arkosic sandstone that contains uranium of economic value (Heinrich, 1958). Clays are primarily montmorillonite and mixed-layer chlorite-montmorillonite (Santos, 1970; Brookins, 1982). This unit contains the Poison Canyon Sandstone (which crops out in Poison Canyon 5 miles north of the GRP site), which contains ore characterized by a uranium-vanadium ratio of 0.5:1, plus coffinite, pyrite, galena (PbS), metatyuyamunite (calcium uranium vanadate), autunite (uranium phosphate), gypsum, kaolinite, calcite, and asphaltite (Heinrich, 1958). In the Poison Canyon Mine, uraninite has been documented (Granger, 1963). Clay in the Poison Canyon unit is dominated by kaolinite and is virtually absent of illite (Brookins, 1990). Poison Canyon's high uranium and very high selenium content (Heinrich, 1958; Brookins, 1982; Chenoweth and Holen, 1980; McLemore, 2010) have made it a target for mining and have provided a source of uranium and selenium to groundwater (Gallaher and Cary, 1986).

The Dakota Sandstone is a fine- to medium-grained quartz sandstone that generally contains no feldspar (Maxwell, 1982). Uranium is present in tabular masses associated with carbonaceous shales or lignite (Granger, 1963), or in fractures in contact with the underlying Brushy Basin Member of the Morrison Fm. (McLemore, 2007).

The Mancos Shale currently only crops out in the upper Basin and in limited extent on the eastern bluffs leading up to Mount Taylor, located 8 miles to the northeast. The Mancos Shale consists of sandstones with thick interbeds of gray shale (Thaden et al., 1967). The extent that the Mancos Shale contributed to the alluvial fill of the lower Basin is unknown.

The deepest units that crop out in the valley are the Triassic Chinle Fm., with low uranium concentrations, which forms the shale and sandstone bedrock beneath the alluvial fill of the lower Basin, and the Triassic Wingate Sandstone, which consists of white quartz eolian sandstone and siltstone that crops out at the base of the bluffs surrounding the valley. Other units that lack significant uranium content include the Jurassic Entrada Sandstone (eolian quartz sandstone/siltstone), Summerville Fm. (clean, white quartz sandstone), and the Bluff Sandstone (clean quartz eolian sandstone). None of the units from the Chinle Fm. to the Mancos Shale have been noted to contain appreciable feldspar except the Morrison Fm. Westwater Canyon and Brushy Basin Members, and small amounts in the Dakota Sandstone.

1.3. Sorption and solubility of uranium and other roll-front geochemical markers

Uranium's association with reduced phases, such as pyrite, mackinawite, siderite, and organic carbon, makes it susceptible to release through reaction with oxidants such as dissolved oxygen in groundwater. Release as U(VI) may be followed immediately by sorption onto oxidized iron minerals (e.g., ferrihydrite or goethite; Dodge et al., 2002). Dissolution of this surface-bound uranium is dependent on displacement through surface chemical reactions. Uranium can be stored in reduced minerals, sorbed to oxidation products, and dissolved through surface desorption reactions, leading to the slow release of uranium from minerals to groundwater. The rate of desorption of uranium from mineral surfaces varies based on geochemical parameters such as carbonate concentration, pH, and total dissolved solids (TDS). Liu et al., 2009, used a multi-rate surface complexation model to simulate desorption kinetics and found that greater desorption occurs in the presence of higher TDS and carbonate.

Higher alkalinity and pH negatively influence uranium sorption through the formation of uranium carbonate complexes (e.g., highly soluble UO_2CO_3, $UO_2(CO_3)_2^{2-}$ and $UO_2(CO_3)_3^{4-}$) (Langmuir, 1978). Solubility is enhanced further in the presence of calcium due to the formation of calcium-uranium-carbonate complexes. These complexes are even more stable in the aqueous phase than uranium carbonate complexes (Stewart et al., 2010). Once formed, each of these complexes increases the mobility of dissolved uranium by limiting uranium sorption to mineral surfaces (attenuation).

Vanadium, molybdenum, and selenium are also affected by redox conditions and are generally more mobile under oxidizing conditions. Vanadium has the lowest solubility of these constituents, with soluble species dominated by V(V) as $H_2VO_4^-$ or HVO_4^{2-}. Lower valence states such as V(IV) and V(III) tend to be more strongly associated with oxides and have lower solubility (Wright et al., 2014). Molybdenum (primarily as MoO_4^{2-}) attenuates through sorption and precipitation under reducing conditions (Smedley and Kinniburgh, 2017). Selenium is released to groundwater primarily through dissolution as selenate (SeO_4^{2-}) as has been documented in the Mancos Shale, where it is liberated from sodium selenate salts and selenium-containing gypsum (Mast et al., 2014).

1.4. Uranium milling and impacts to groundwater by the Homestake and Bluewater Mills

The Grants-Ambrosia Lake uranium mining district in northwestern New Mexico produced more uranium than any other mining district in the United States between 1951 and 1980 and continues to be an area of exploration and plans for development (McLemore, 2007). The Grants district is located within the Colorado Plateau, an area of approximately 150,000 square miles, exposing the Cretaceous and Jurassic strata and an abundance of economically viable mineral deposits including uranium and vanadium, as well as copper, silver, gypsum, coal, and oil shale (Heinrich, 1958). Mining of uranium deposits in the district began in earnest with the start of the U.S. Atomic Energy Commission's domestic uranium program in 1948. Uranium ore from Ambrosia Lake was milled at four facilities. Two are located at the southern terminus of the Basin: the Anaconda Bluewater Mill and the Homestake Mill. The Bluewater Mill, located west of the GRP, was built in 1953 to process ore from the Todilto Limestone (carbonate leach) and Jackpile Mine (acid leach) (McLemore, 2010) and closed in 1982 (McLemore, 2007). The mill was transferred from the Atlantic Richfield Company (ARCO) to the U.S. Department of Energy Office of Legacy Management in 1997 (U.S. Department of Energy (USDOE, 2014). Seepage from the 22.9 million tons of tailing at the Bluewater Mill have affected the Rio San Jose alluvial aquifer and the San Andres-Glorieta aquifer, a major water source for irrigation and municipal supply in the region (U.S. Department of Energy (USDOE), 2014).

The Homestake Mill, the focus of the GRP, is located 5.5 miles north of Milan, was built in 1957, and was decommissioned in 1990. The Homestake Mill currently is undergoing closure with a focus on restoring groundwater affected by seepage from an unlined impoundment (the Large Tailing Pile [LTP]) composed of 21 million tons of tailing from an alkaline (sodium carbonate) leach milling process (Homestake Mining Company (HMC), 2012). Groundwater quality in the alluvial aquifer and other aquifers at the GRP is being restored by extraction of groundwater, reinjection to provide hydraulic damming and enhance flushing of the aquifer, and treatment through reverse osmosis and zeolite systems to meet restoration goals established by the NRC, New Mexico Environment Department, and USEPA. Groundwater restoration of the alluvial groundwater system will be complete when the Groundwater Protection Standards (GWPS) for individual constituents are achieved; the majority of these standards are based upon a study of alluvial groundwater quality upgradient of the GRP during the period 1995–2004 (NRC, 2006) to ensure that the standards are representative of the natural alluvial system. GWPS for uranium, nitrate, selenium, sulfate, TDS, thorium-230, and vanadium are based on their background concentration in the lower Basin alluvial aquifer upgradient of the GRP site. The GWPS for molybdenum, chloride, and combined radium-226/radium-228 are based upon EPA water quality standards or guidance. The EPA and NMED water quality standard for uranium is 0.03 mg per liter (mg/L; U.S. Federal Code of Regulations; New Mexico Administrative Code), and the background concentration of uranium at the GRP is 0.16 mg/L.

1.5. Dual-domain Source of inorganics

This work investigates the source of inorganic constituents to groundwater from lower permeability materials in the aquifer system where diffusion is the dominant constituent transport mechanism (as opposed to advection-dominated high permeability materials). Various studies discussed below show that uranium in natural systems characterized by fine-grained, low-permeability sediments undergoes cycles of storage and release, providing a constant source of uranium to groundwater. Advective processes in the large pore spaces of high hydraulic conductivity sediments facilitate groundwater mixing, while mixing is limited in the small pore spaces of low-permeability sediments. Consequently, the accumulation of uranium in groundwater in low-permeability sediments is a greater expression of geochemical characteristics immediately adjacent to the sampling point (well), while advection-dominated flow

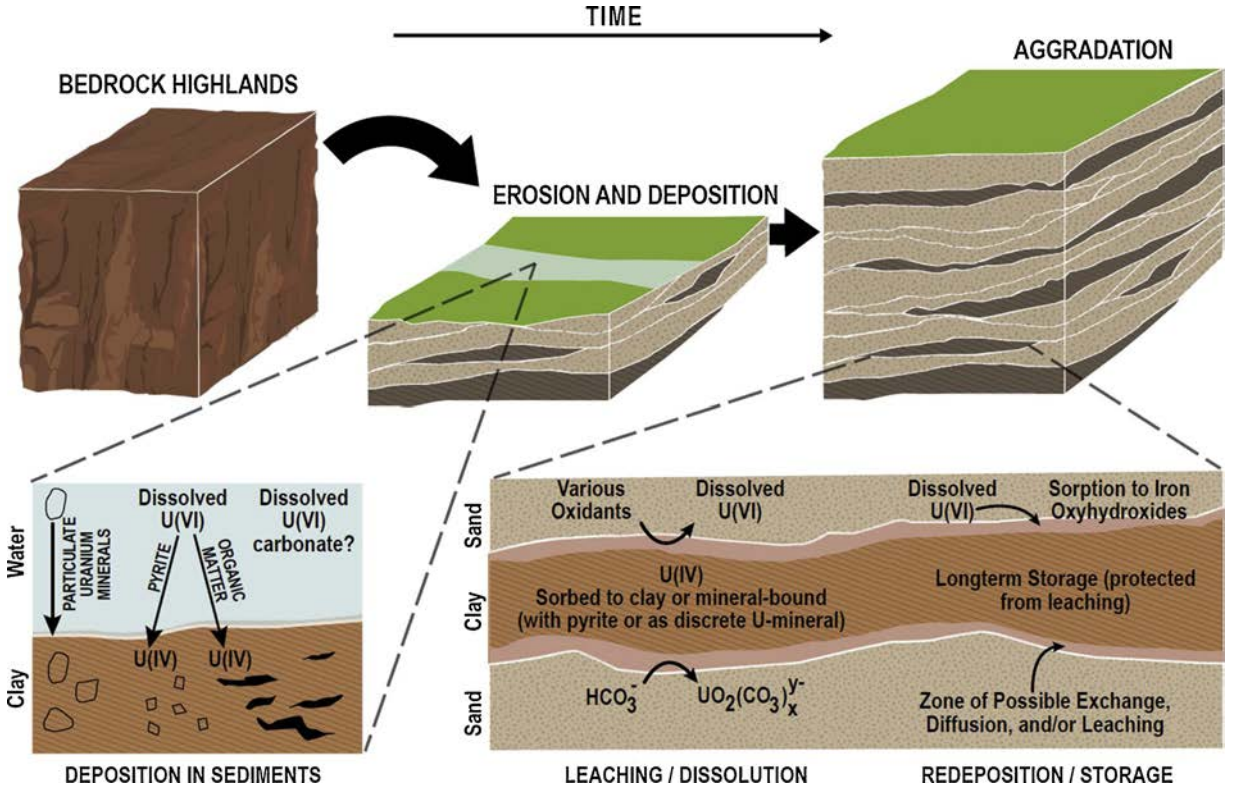

Fig. 3. Conceptual model of formation of uranium-bearing alluvium and cycling of uranium between clays and sands after deposition. The bedrock highlands depicted here represent key uranium-containing units in the Basin such as the Morrison Fm. and Dakota Sandstone.

through coarser-grained sediments is more representative of groundwater characteristics that have been averaged over a larger area. The conceptual model presented in this paper in Fig. 3 shows: 1) weathering of bedrock-hosted uranium deposits and transport and deposition of naturally uranium-bearing sediments providing a source of uranium to the alluvium at and upgradient of the GRP and 2) processes that occur at the interface of low- and high-permeability sediments resulting in local, fine grain sediment-sourced uranium into groundwater.

Uranium's dynamic geochemical behavior is rendered even more complex in saturated aquifer sediments composed of multiple hydraulic domains such as those that exist at the GRP. At the large scale, groundwater flow and solute flux in an alluvial aquifer is dominated by advection through the most permeable materials (in the case of the lower Basin, this is the sand- and gravel-dominated strata); however, finer-grained sediments (e.g., silts and clays) contain porosity that is accessed only through diffusion. Fine-grained, low-permeability sediments have been shown to accumulate uranium from groundwater in aquifer systems where uranium is present as a contaminant. Lefebvre et al. (2019) studied the cycling of uranium in the Upper Colorado River Basin, with a focus on the presence of naturally reduced zones (NRZs) established in fine-grained material (< 150-micron [μm] grain size) containing reduced iron minerals. The authors concluded that these NRZs constitute a significant source of uranium to pore water through oxidation of uranium and release to surrounding high-permeability zones in coarse-grained sediments. At Riverton, Wyoming, a legacy mill tailings site managed by the USDOE, uranium in groundwater was found to be retained in silts and released to groundwater in sands and gravels, resulting in a persistent uranium plume in the aquifer downgradient from the mill (Johnson et al., 2018). In both cases, uranium in groundwater was derived from seepage from mill tailings and bore the chemical signature of this seepage in terms of major and trace element composition. Sampling locations for the work presented in this paper are upgradient of the GRP and did not show evidence of mill-related contamination; however, the principles of cycled liberation and sequestration of uranium apply. In fact, Johnson et al. (2018) also saw release of uranium, sulfate, and chloride from a location outside of their contaminant plume and concluded that the release of these constituents was "a naturally occurring process."

A study in the Jacobsville Sandstone in Michigan's Upper Peninsula combined the evaluation of groundwater quality, $^{235}U/^{238}U$ isotope ratios, and geophysical logging of wells to develop an understanding of the presence of uranium in groundwater at concentrations exceeding 30 μg per liter (μg/L) at locations outside of mining or milling influence (Sherman et al., 2007). Uranium-bearing unconsolidated strata were identified through geophysical methods to be clay-dominated and laterally contiguous over tens of meters. Groundwater in contact with these clay-dominated strata showed elevated concentrations of uranium. Uranium associated with heavy minerals, such as thorium, in shale were less readily leached due to uranium's lower solubility when complexed with thorium and due to the lower permeability of the shales. Elevated concentrations of uranium in the oxidized, alkaline aquifer were attributed to dissolution of secondarily precipitated uranium minerals in the clay and unconsolidated sandy sediments in the area

(Sherman et al., 2007).

The Tono uranium deposit in Japan is a fluvial lignite-bearing formation containing uranium due to reducing conditions induced by lignite and pyrite (Yoshida et al., 1994). Uranium in these sediments was found in association with framboidal and micro-subhedral pyrite as well as with biotite in clays. Uranium concentrations are relatively low in groundwater at 0.05 to 0.2 µg/L due to the low permeability of the sandstone and very low TDS (< 100 mg/L) and alkalinity (~80 mg/L). Unlike most studies investigating the source of uranium to groundwater, the low-permeability, deep anoxic groundwater system here does not show a redox transition at the interface of the fine- and coarse-grained sediments; consequently, the dissolution of uranium from host mineral phases is limited.

Uranium in a Quaternary aquifer system of the Datong basin in China, where the concentration of geogenic uranium in sediments ranged from 1.9 to 8.8 mg/kg (highest concentrations were present in the finer-grained sediments) was shown to contribute uranium to shallow groundwater at concentrations up to 119 to 209 µg/L. This work demonstrated the importance of oxidation process and weather of uranium-bearing minerals by bicarbonate (with the formation of calcium-uranium-carbonate complexes predicted through geochemical modeling)(Wu et al., 2019).

The above summary of the variable occurrence of chemical forms of uranium relevant to ore formation and subsequent weathering, erosion, and deposition, and the dynamic nature of uranium mobility influenced by geochemical conditions of the groundwater system, were evaluated within the groundwater system in the Grants region and lower SMCB. The hypothesis guiding this work is that uranium in groundwater upgradient from the mill is naturally-sourced from the alluvial sediments and the background concentration is affected by variability in lithology, mineralogy, and groundwater chemistry within the system.

2. Methods

2.1. Sediment sampling and analysis

In January 2018, two boreholes were completed using rotosonic drilling adjacent to existing upgradient wells DD and DD2 in the background area at the GRP (Fig. 4). Detailed boring logs were completed for the alluvial materials, with boreholes drilled down to and a short distance into Chinle Fm. shale bedrock to 85 feet bgs total depth for borehole DD-BK (~10 feet southeast of well DD) and 100 feet bgs at borehole DD2-BK (~40 feet northeast of well DD2). Cores were recovered, staged on plastic tarps, and covered when

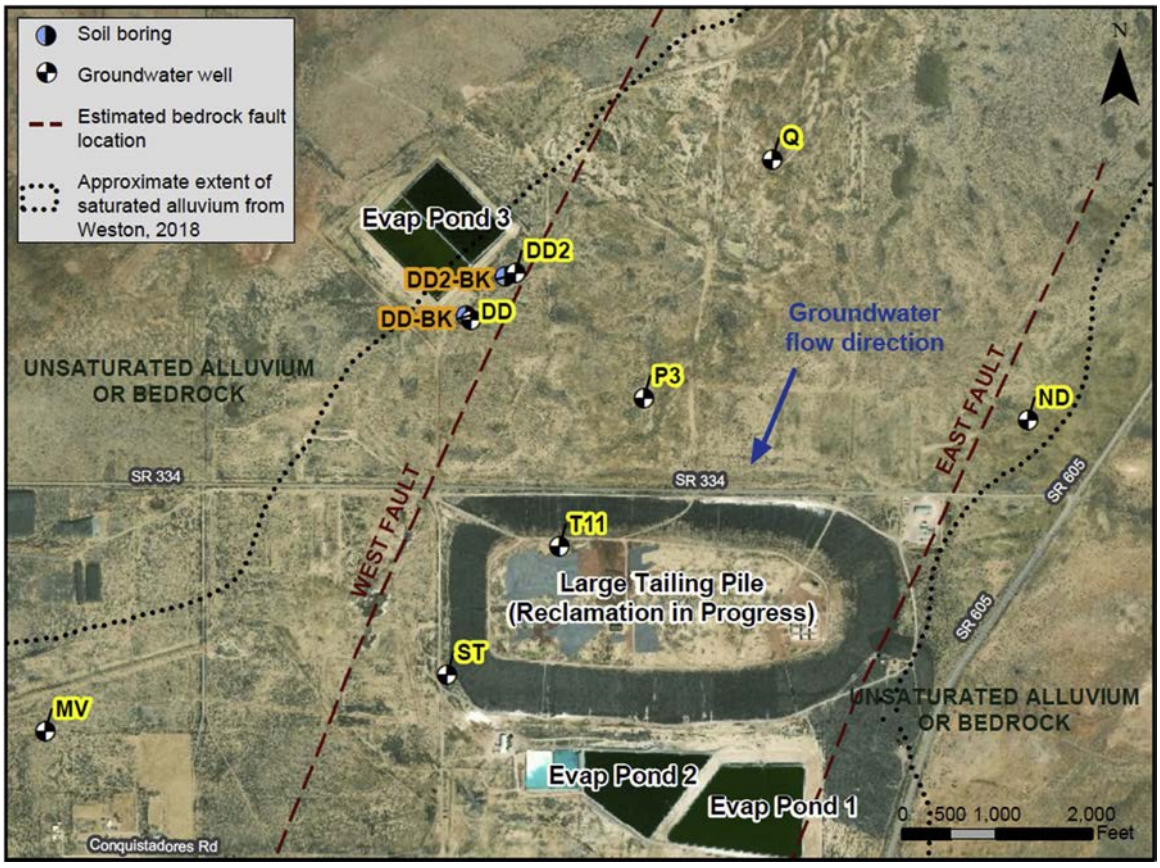

Fig. 4. Locations of wells and boreholes.

not in use. The boreholes were completed as blank wells with Schedule 40 polyvinyl chloride (PVC) risers (no screen). Downhole geophysical methods were conducted before selection of soil samples. Ten soil samples were collected from borehole DD-BK, and nine samples plus a duplicate were collected from borehole DD2-BK. Samples were selected to obtain representative coarse- and fine-grained soil types and were guided by the results of the geophysical analyses. Uranium (U), major elements (aluminum [Al], iron [Fe], sodium [Na], potassium [K], phosphorus [P]), and trace elements (molybdenum [Mo], selenium [Se], vanadium [V]) were analyzed at Energy Laboratories, Inc. in Casper, Wyoming by USEPA Method 3050B (hydrochloric/nitric acid digestion) and USEPA Method 6020B (inductively coupled plasma mass spectrometry [ICP-MS]). The leachability of uranium and trace elements were evaluated by USEPA Method 1312, modified with an alkaline extractant in lieu of the standard acidic extractant per Kohler et al. (2004). Five samples from DD-BK and four from DD2-BK were analyzed by ACZ Laboratories in Steamboat Springs, Colorado for grain size distribution by hydrometer (ASA No. 9, Pt. 1, Section 15–5). Based on the results of the total uranium analysis, eight samples were selected and sent to DCM Science Laboratory (Lakewood, Colorado) for optical evaluation of mineralogy using a Leitz Ortholux POL-BK petrographic microscope and scanning electron microscopy with energy-dispersive x-ray spectroscopy (SEM-EDS) via Field Emission Scanning Electron Microscope (TESCAN). Standard thin sections could not be prepared on a number of the samples due to the high swelling clay content; in these cases, polished billets were carbon-coated for analysis by SEM-EDS. Six samples were evaluated by powder x-ray diffraction (XRD) on a Phillips XRG 3100 X-ray diffractometer. XRD was conducted over a range of 4° to 45° 2Θ Cu Kα radiation, 40 kV, 25 milliamperes. Estimates of mineral concentrations were based on relative peak heights and reference intensity ratios. Clay-specific XRD was conducted on two samples by segregating the < 2 μm size fraction through suspension in water, centrifugation, filtration, and mounting of the clay slab caught on the filter.

2.2. Geophysical assessment (2016 and 2018)

USGS conducted a geophysical logging event from August 8 through 13, 2016 at six monitoring wells completed in the alluvial aquifer (DD, DD2, MV, ND, Q, T11; Harte et al., 2019). Geophysical techniques included measurement of well construction and integrity (caliper, optical televiewer), groundwater/aquifer physical characteristics (induction, electromagnetic (EM) flowmeter, fluid temperature, and conductivity), and radioactivity of the material surrounding the well (natural gamma ray and natural gamma ray spectroscopy). USGS performed pumped flow meter testing in three of the six wells (DD, ND, and Q).

As part of the follow-on study presented here, boreholes DD-BK and DD2-BK were evaluated using downhole geophysical methods including natural gamma ray, natural gamma ray spectroscopy, and induction conductivity. Matrix Logger Version 10 software was used to log data from the Mount Sopris Instruments geophysics package including: a) 2PGA-1000 1.63 in. dia. × 31.3 in. sodium iodide-thallium (NaI(Tl)) natural gamma scintillometer; b) 2SNA-1000S 1.5 in. × 46.6 in. temperature compensated NaI(Tl) spectral gamma scintillometer; and c) a 2EMA-1000 1.44 in. × 66.9 in. induction conductivity probe (39.2 kHz operating frequency).

Natural gamma ray and induction conductivity logging were completed in a single, continuous pass at an approximate logging speed of 12 feet per minute. Natural gamma ray spectroscopy logging was performed in two modes: dynamic (3 feet per minute downward and upward) and static at pre-selected depths. The dynamic data were reviewed in the field to select the static measurement depths; each static measurement was made over a 15- to 20-minute period to ensure that a statistically significant integrated value would result. The natural gamma ray spectroscopy data collected from boreholes DD-BK and DD2-BKwere modeled in WellCAD to calculate the estimated uranium, thorium, and potassium content of the alluvium at specific static measurement depth intervals. The spectral stripping method was used (Ellis and Singer, 2008), and a specific calibration model for the logging probe was used to calculate the weight-based concentrations. Borehole geophysical graphic logs were produced using WellCAD portraying the geophysical results, visual lithology descriptions, and relevant analytical results.

2.3. Groundwater sampling and analysis

In August 2016, groundwater samples were collected from 8 alluvial wells immediately surrounding and on the site, capturing a range of groundwater quality across the GRP, including background wells. The six alluvial monitoring wells that were subjected to geophysical logging (DD, DD2, MV, ND, Q, and T-11) were also sampled through passive diffusion samplers (PDS) and micropurge (MP) methods, in addition to the conventional pumping (volumetric purge [VP]) sampling techniques (Harte et al., 2019; Table 1). This paper focuses on the results from the VP. Split (duplicate) samples were collected concurrently at each location by the USGS and Homestake Mining Company (HMC) and excepting stable sulfur isotope analyses, they were analyzed separately at different laboratories, resulting in two datasets. The data presented here are results from the HMC samples as these are the data collected by the authors. The USGS data are generally comparable and are presented in a number of reports and publications (Blake et al., 2019, Harte et al., 2018 and references therein). Static water level measurements were collected before sampling. Field parameters (temperature, pH, specific conductance, dissolved oxygen [DO], turbidity, and oxidation-reduction potential [ORP]) were measured using a single in-line flow-through cell and recorded by both the USGS and HMC. DO and ferrous iron were measured using a Hach DR1900 Portable Spectrophotometer with Hach Methods 8166 and 8146, respectively. For passive sampling, groundwater samples were collected using nylon screen PDSs per Vroblesky et al. (2002, 2003). USGS increased the PDS size from the 30-milliter (mL) used by Vroblesky et al. (2002, 2003) to 250 mL (U.S. Geological Survey (USGS), 2016a, 2016b), which may have affected the PDS functionality (HMC, 2018). Details on methods and results from PDS analyses are provided in HMC, 2018; Harte et al., 2019; and Blake et al., 2017.

Table 1
Well and Borehole Construction Details for 8 Alluvial Aquifer Wells and Boreholes, Grants Reclamation Project.

Location	Well or Borehole	Type of sampling conducted	Downhole geophysics conducted	Latitude	Longitude	Location	Total depth (ft bgs)	Well screen interval (ft bgs)	Predominant lithology in screened interval	Constituent concentration, VP October 2016 (mg/L unless otherwise noted)			
										Molybdenum	Selenium	Uranium	Vanadium
Q	Well	GW: VP, MP, PDS	Yes	35°15' 24.069" N	107°51' 34.626" W	~0.7 miles N of LTP	100.5	67.5-100.5	Gravel	D: 0.002 T: 0.002	D: 0.416 T: 0.38	D: 0.0523 T: 0.0525	D: 0.00056 T: 0.00048
P3	Well	GW: VP	No	35°14' 58.995" N	107°51' 51.106" W	~0.2 miles N of LTP	95.0	55-95	Tan sand, gravel, clay, and red shale	D: 0.001 T: 0.002	D: 0.276 T: 0.254	D: 0.0201 T: 0.0209	D: NA T: 0.00043
DD	Well	GW: VP, MP, PDS	Yes	35°15' 7.202" N	107°52' 13.318" W	~0.4 miles NNW of LTP	80.0	42-80	Medium sand, red clay, coarse sand and gravel	D: 0.002 T: 0.001	D: 0.114 T: 0.103	D: 0.0944 T: 0.0869	D: 0.00025 T: 0.01
DD2	Well	GW: VP, MP, PDS	Yes	35°15' 12.160" N	107°52' 7.574" W	~0.5 miles NNW of LTP	92.5	54-90	Red and grey shale, sand, and gravel	D: 0.001 T: 0.001	D: 0.0005 T: 0.00057	D: 0.218 T: 0.221	D: 0.00044 T: 0.01
ND	Well	GW: VP, MP, PDS	Yes	35°14' 56.715" N	107°51' 1.826" W	~0.4 miles NE of LTP	68.7	41.5-61.5	Gravel, sand, and Chinle	D: 0.005 T: 0.005	D: 0.131 T: 0.115	D: 0.0195 T: 0.0188	D: NA T: 0.0075
ST	Well	GW: VP	No	35°14' 29.869" N	107°52' 16.375" W	SW side of LTP	97.0	55-97	–	D: 6.8 T: 7.58	D: 0.176 T: 0.153	D: 4.49 T: 4.82	D: 0.0023 T: 0.0027
T11	Well	GW: VP, MP, PDS	Yes	35°14' 43.424" N	107°52' 1.925" W	Alluvium beneath LTP	193.0	113-193	Tan sand, gravel, cobbles, clay, and shale	D: 23.2 T: 23.4	D: 0.144 T: 0.151	D: 8.39 T: 8.22	D: 0.09 T: 0.09
MV	Well	GW: VP, MP, PDS	Yes	35°14' 23.943" N	107°53' 7.859" W	~0.9 miles WSW of LTP	105.2	75.5-105	Fractured basalt and sand	D: 0.02 T: 0.021	D: 0.033 T: 0.031	D: 0.249 T: 0.242	D: 0.0018 T: 0.002
DD-BK	Borehole	Lithological	Yes	35° 15' 7.189" N	107° 52' 15.632" W	~0.4 miles NNW of LTP	85	–	–	0.0049 mg/kg	0.0021 mg/kg	0.0057 mg/kg	0.073 mg/kg
DD2-BK	Borehole	Lithological	Yes	35° 15' 12.222" N	107° 52' 11.586" W	~0.5 miles NNW of LTP	100	–	–	0.013 mg/kg	0.0027 mg/kg	0.035 mg/kg	0.052 mg/kg

Notes: – Not applicable; ft amsl - feet above mean sea level; ft bgs - feet below ground surface; GW – groundwater; LTP - Large Tailing Pile; MP - micropurge groundwater sampling; data not presented; PDS - passive diffusion groundwater sampling; data not presented;VP - volumetric purge groundwater sampling; Lithological - solid sampling of core with geochemical and mineralogical analyses (detailed in text); D - Dissolved analysis (filtered with 0.45 μm filter); T - Total analysis (unfiltered); Bottom of screen interval used if total depth is less than screen interval.

VP samples were collected after three well casing volumes were purged. VP samples were analyzed for several constituents including but not limited to various major and trace metals, major anions and cations, and stable sulfur and uranium isotopic analysis (Table 1).

3. Results

3.1. Geophysical assessment and lithological logging

The combination of detailed core logging and geophysical methods yields a high-resolution picture of the subsurface that included alternating lenses of silty sands and clays of various thicknesses, ranging from less than 1 foot to greater than 20 feet. Abrupt changes in lithology type (e.g., gravel to silty-clay) with depth are observed (see geophysical logs in Supplemental S-1 and boring logs in Supplemental S-2). Core logging indicates that coarse-grained intervals are composed primarily of sand, with trace gravel localized in thin layers. Clay layers range from 0.5 inch to several feet in thickness and are generally hard, with moderate to high plasticity. Results from particle size analysis conducted on eight samples corroborate the field observations. The coarser-grained soils are sub-rounded to angular. Coarse-grained layers often contain fines and clay materials, sometimes cementing lithic fragments of varying color (Fig. 5).

Results of the geophysical assessment of the six existing wells and two new boreholes indicate that the central portion of the alluvial channel has more coarse-grained material compared to the flanks of the alluvial channel. Well locations within the center of the channel exhibit a lower uranium concentration in sediment, and the association between coarse grain size and lower uranium content is discernible. In contrast, the wells at the flanks of the valley have more fine-grained materials and exhibit a higher frequency of elevated readings of uranium. In wells DD and DD2 on the western margin of the alluvial channel, there are several uranium concentration peaks in the sediments in the screened interval. The localized concentration of uranium in the sediment layers near DD and DD2 results in differences in uranium concentration in groundwater.

The thorium-potassium ratio can be used to estimate the types of clay minerals present and infer the relative maturity of sediments. A ratio less than 0.3 indicates that the source of radioactive potassium is primarily found in potassium feldspars and potassium-bearing evaporite minerals. Progressively higher ratios signal transition from detrital micas (glauconite is only found as an authigenic marine clay and is not relevant here), illite, mixed layer clays (illite-montmorillonite), and chlorite and kaolinite. A majority of the samples exhibit mixed-layer clay characteristics, which supports the petrographic microscopy and SEM results.

3.2. XRD and petrographic and scanning electron microscopy

XRD was completed on six samples. Two of these samples received both bulk mineralogy XRD and clay-specific XRD. The general characteristics for both fine- and coarse-grained sediments include ubiquity of fine-grained materials, mixtures of oxidized and reduced-phase minerals (e.g., sulfates/oxides and sulfides), and widespread presence of iron oxides. The clay XRD results indicate that the clays consist of smectite, illite, and kaolinite, and microscopy shows that clays frequently contain organic material and amorphous iron oxide, pyrite, and framboidal pyrite pseudomorphs as iron oxides. Both XRD and microscopy show that the majority of the non-clay material is quartz, potassium feldspar, and plagioclase, representing erosion and weathering products from arkosic sandstones (granites are not prevalent in the area), and occasional indications of basalt and other volcanics including volcanic glass. Clay is observed as a cementing agent for fine-grained quartz and feldspar (Fig. 5B, 5D), and as a coating for larger silicate fragments. Occasionally, calcite, gypsum, and hematite are detected through XRD and microscopy. Visual observation by the laboratory suggests that up to 3% of the material is iron oxide due to the red color of the samples; as this is not seen in the XRD spectra, the iron oxide is assumed to be amorphous. Most samples contain pyrite framboids and/or iron oxide pseudomorphs of pyrite framboids (Fig. 5F) and organic carbon (Fig. 5A, 5B). Feldspar is detected in six samples. Volcanic glass is observed in one sample in borehole DD2-BK at 25–26 feet bgs.

Vanadium is detected in the EDS analysis. Soil from both DD2-BK at 25 to 26 feet bgs and 60 to 61 feet bgs show a clay mass with vanadium and rare-earth elements. This sample contains ~32 mg per kilogram (mg/kg) vanadium, one of the highest concentrations measured in this study. Vanadium in soil is generally present at much higher concentrations (10 to 15x) than uranium. Uranium is not detected in the samples by SEM-EDS. This could be due to two factors: 1) either the uranium is segregated into discrete mineral phases (such as uraninite) and the probability of encountering one of these mineral fragments is very low or 2) the uranium is so finely disseminated throughout the sample that it occurs in concentrations below the detection limit of the EDS (i.e., it is present at a concentration less than 1000 ppm [0.1 wt. % or 1000 mg/kg] in any one area). Automated EDS mapping was not performed; this approach may have enabled detection of uranium if detection is predominantly limited by factor 1. While uranium and vanadium are often associated in environmental samples, vanadium is typically less soluble than uranium, and it does not form soluble complexes with carbonate (Wright et al., 2014), which could explain why solid vanadium was seen in these samples via SEM-EDS and uranium was not. While uranium may oxidize and dissolve in pore water, vanadium may be more strongly retained and preserved at higher concentrations in the soils (Telfeyan et al., 2015).

3.3. Bulk chemistry

The highest uranium concentrations (1–10 mg/kg) generally occur in fine-grained materials including clay, silt, and silty fine sands (Table 2). In one case, a gravelly sand with silt contained 5 mg/kg uranium. Higher uranium concentrations are associated with

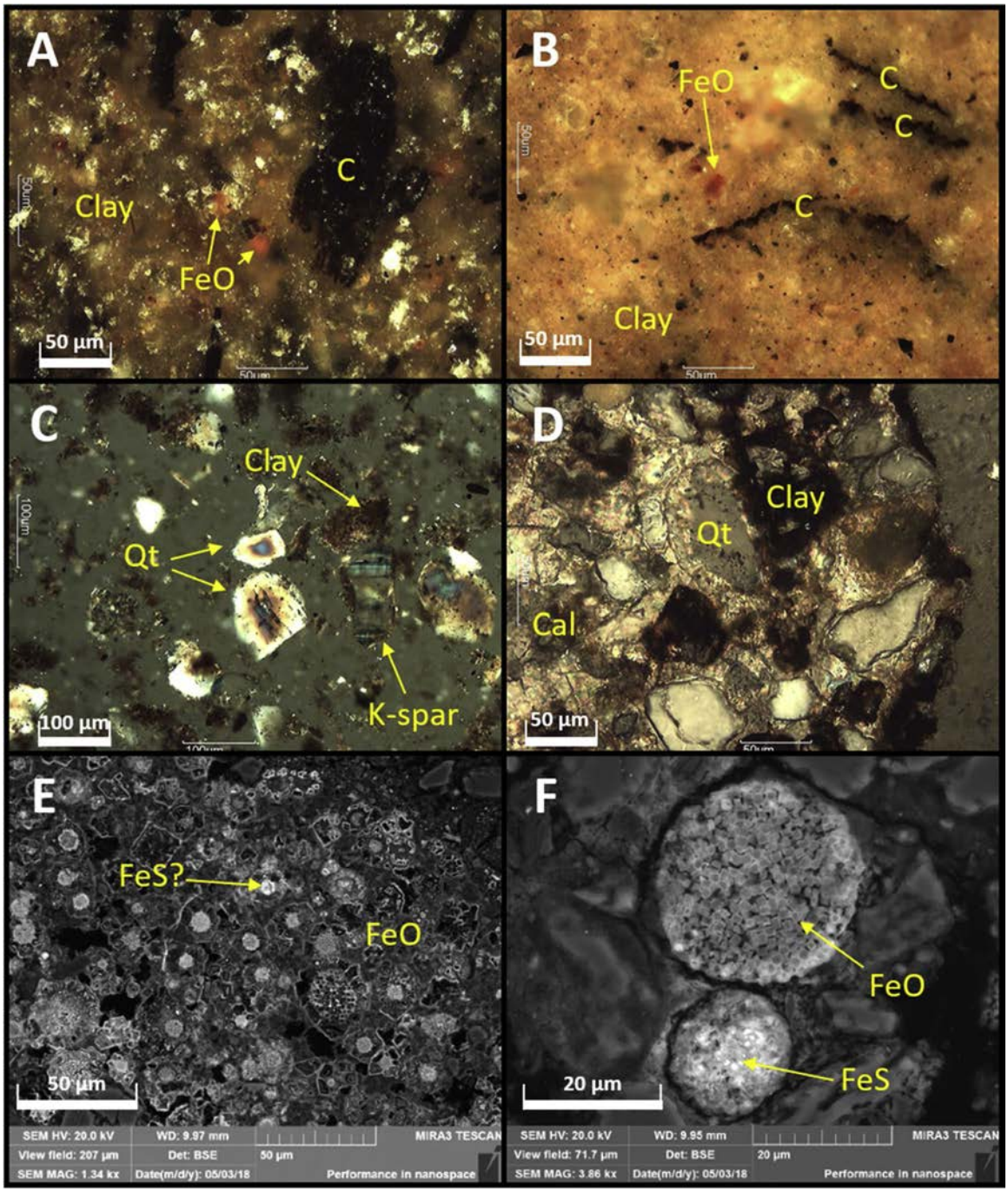

Fig. 5. Petrographic and scanning electron microscopy images by DCM Science Laboratory in Wheat Ridge, Colorado. C - carbon, Cal -calcite, FeO – iron oxide, FeS – iron sulfide, K-spar – feldspar, Qt – quartz. A) Clay with black carbon and red iron oxide in DD-BK at 9–10 feet bgs (unsaturated). Reflected light crossed polars 200 × . B) Clay with **black** organics and small grains of iron oxide in DD2-BK at 11–12 feet bgs. Reflected light crossed polars 200 × . C) Sand sized particles of quartz/feldspar grains and dark clay in DD-BK at 36–37 feet bgs (unsaturated). Polarized light 100 × . D) Quartz/feldspar grains with calcite and iron oxide cement in DD2-BK at 25–26 feet bgs (unsaturated). Reflected light crossed polars 200 × . E) Iron oxide pseudomorphs of pyrite cubes and framboids in DD2-BK at 25–26 feet bgs (unsaturated). Backscatter scanning electron micrograph, 1,340 × . F) Iron oxide pseudomorphs of pyrite framboids in a matrix of clay with quartz/feldspar grains in DD2-BK at 51-51 feet bgs (saturated). Backscatter scanning electron micrograph, 3,860× (For interpretation of the references to colour in this figure legend, the reader is referred to the web version of this article).

Table 2
Bulk Chemistry and Leach Test Data for Solid Samples from Boreholes DD-BK and DD2-BK, Grants Reclamation Project.

Borehole	Depth (fbgs)	Total metals - EPA Method 3050B/6020B (mg/kg dry mass)				Synthetic precipitation leaching procedure[a] (mg/L)				Lithology as Logged in the Field
		Molybdenum	Selenium	Uranium	Vanadium	Molybdenum	Selenium	Uranium	Vanadium	
DD-BK	9-10	< 1 U	< 1 U	1	26	0.002	0.002	0.0022	< 0.01 U	Clay with trace sand
	15-16	< 1 U	< 1 U	< 1 U	7	0.002	< 0.001 U	0.0018	0.07	Fine to medium sand with some silt
	27-28	< 1 U	< 1 U	< 1 U	5	0.004	< 0.001 U	0.0012	0.03	Fine to coarse sand with trace silt
	30-31	< 1 U	< 1 U	< 1 U	12	0.005	0.002	0.0032	0.07	Silty sand and gravel
	36-37	< 1 U	< 1 U	1	15	0.005	0.005	0.0127	0.1	Clay
	39-40	1	< 1 U	< 1 U	9	0.014	0.002	0.007	0.13	Silty sand with hard layer
	50-51	< 1 U	< 1 U	< 1 U	7	0.004	< 0.001 U	0.0059	0.06	Silty fine to coarse sand
	58-59	< 1 U	< 1 U	1	34	0.003	0.002	0.0032	0.03	Clay
	63-64	< 1 U	< 1 U	< 1 U	11	0.004	0.002	0.0075	0.13	Silty fine sand
	66-67	< 1 U	< 1 U	< 1 U	13	0.006	0.003	0.0118	0.1	Silty fine sand
DD2-BK	11-12	3	< 1 U	10	34	0.042	0.001	0.179	0.02	Clay
	25-26	< 1 U	< 1 U	1	7	0.033	< 0.001 U	0.0477	0.03	Sand with trace silt
	36-37	< 1 U	< 1 U	< 1 U	8	0.009	0.003	0.009	0.06	Silty fine sand
	51-52	< 1 U	< 1 U	2	15	0.002	0.001	0.0086	< 0.01 U	Silty sand
	56-57	< 1 U	< 1 U	1	29	0.005	0.002	0.0079	0.05	Clay
	60-61	< 1 U	< 1 U	2	32	0.005	0.002	0.0086	< 0.01 U	Clay
	65-66	< 1 U	< 1 U	1	16	0.007	0.001	0.008	0.12	Fine sandy silt
	67-68	< 1 U	< 1 U	1	11	0.007	0.002	0.018	0.12	Silty sand / Clay
	71-72	1	2	5	20	0.004	0.011	0.0305	0.05	Gravely sand with some silt

Notes: [a]Modified synthetic precipitation leaching procedure described within publication; fbgs = feet below ground surface; mg/kg = milligram per kilogram; mg/L = milligram per liter; U = not detected; method detection limit shown.

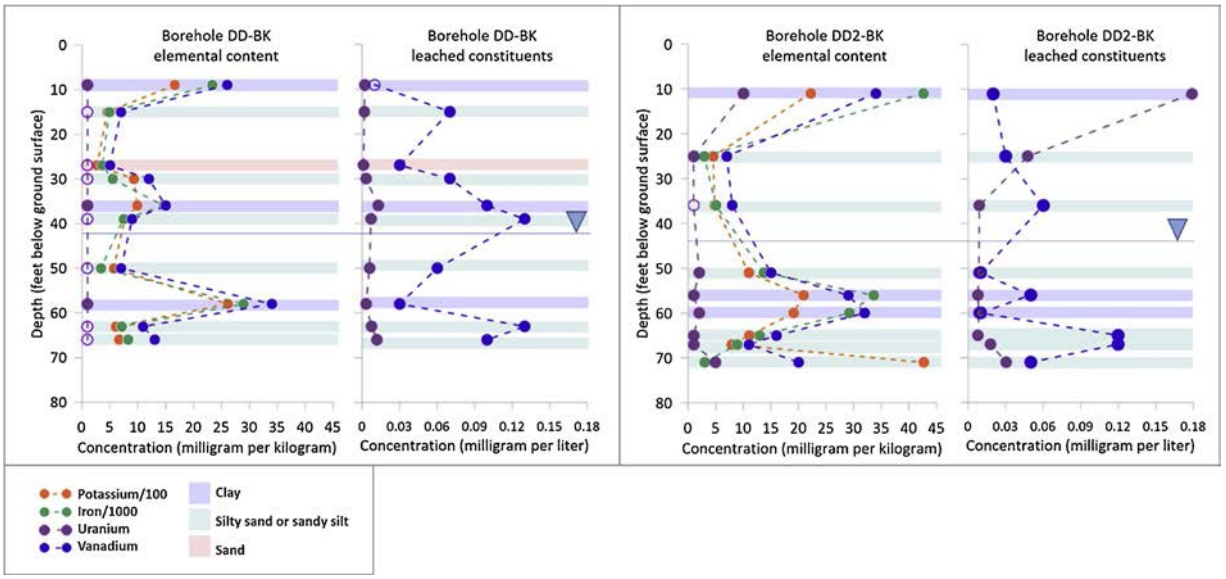

Fig. 6. Sediment total element concentration and leached element concentration results are shown for borehole DD-BK (left) and DD2-BK (right). In order to plot all constituents on the same scale, potassium results have been divided by 100 and iron results have been divided by 1000. Non-detect results are shown as an open circle and displayed at the laboratory reporting limit. Colored bars represent the lithology of each sample; the thickness of the bar is standard for display purposes and does not reflect the thickness of each lithology in the core. For lithological unit thickness, see Supplementary Information S-2.

higher concentrations of aluminum, iron, phosphorus, potassium, sodium, and vanadium (Fig. 6). Metals/metalloids, such as molybdenum and selenium, are not detected during bulk chemistry analysis in most samples but are detected in leached samples, indicating low level presence in samples.

Uranium is detected in samples collected both above and below the water table at each boring, and the highest uranium concentration (10 mg/kg) is measured in clay in the unsaturated zone at 11–12 feet bgs, approximately 30 feet above the groundwater table which varies seasonally between 40–45 feet bgs in this area.

3.4. Leach tests

Leached molybdenum, selenium, and uranium are roughly inversely proportional to the bulk of the total metals concentrations for aluminum, iron, phosphorus, potassium, and sodium at each depth. For samples with high total metals concentration, low to moderate leaching of molybdenum, selenium, and uranium is apparent. Higher uranium and vanadium concentrations are leached from clay and silt-containing samples compared to samples that are primarily sand (Fig. 6). Uranium exhibits a proportional relationship between the leached concentration and the total uranium concentration and is most leachable in the shallowest and deepest samples analyzed (< 36 feet bgs: silty sand and clay, and > 67 feet bgs: silty fine sands). Leach test results for vanadium are highest in samples presenting a higher proportion of silts and do not always reflect the highest total vanadium concentration. Leached selenium is generally detected in samples collected from fine-grained lithologies that exhibit higher iron concentrations and do not always correspond to a higher leached uranium concentration. The presence of molybdenum is generally positively correlated with the presence of higher concentrations of uranium.

3.5. Groundwater results

Stiff diagrams were prepared for each well (Fig. 7). Upgradient alluvial wells DD, DD2, P3, and Q are characterized by high sulfate, moderate calcium, and low chloride. Upgradient alluvial well ND contains about an order of magnitude lower TDS and is characterized by moderate sodium, potassium, and sulfate, and low calcium, magnesium, chloride, and alkalinity. T11 and ST, wells that are affected by site contamination, present the classic “anvil” shape with a high sodium, potassium, and sulfate and moderate amounts of calcium, magnesium, chloride, and alkalinity. Well MV is also known to be affected by the site, but is farther away from the tailings piles and shows lower concentrations of all major ions than wells located close to the piles.

Concentrations of milled uranium ore geochemical markers (tailing-derived uranium, molybdenum, and vanadium) are highest in well T11, which is screened in the alluvium beneath the LTP. Uranium concentrations in the alluvial aquifer vary from 0.0188 mg/L in near-upgradient alluvial well ND to 8.39 mg/L in T11. The uranium concentrations in groundwater at upgradient well ND on the eastern side of the alluvial channel are low when compared to upgradient wells DD (0.0869 mg/L) and DD2 (0.221 mg/L) on the western side of the alluvial channel, demonstrating the local heterogeneity in uranium concentrations across the alluvial channel. Vanadium concentrations are highest at T11 (0.09 mg/L) and low to non-detect at other wells. Previous reports show that

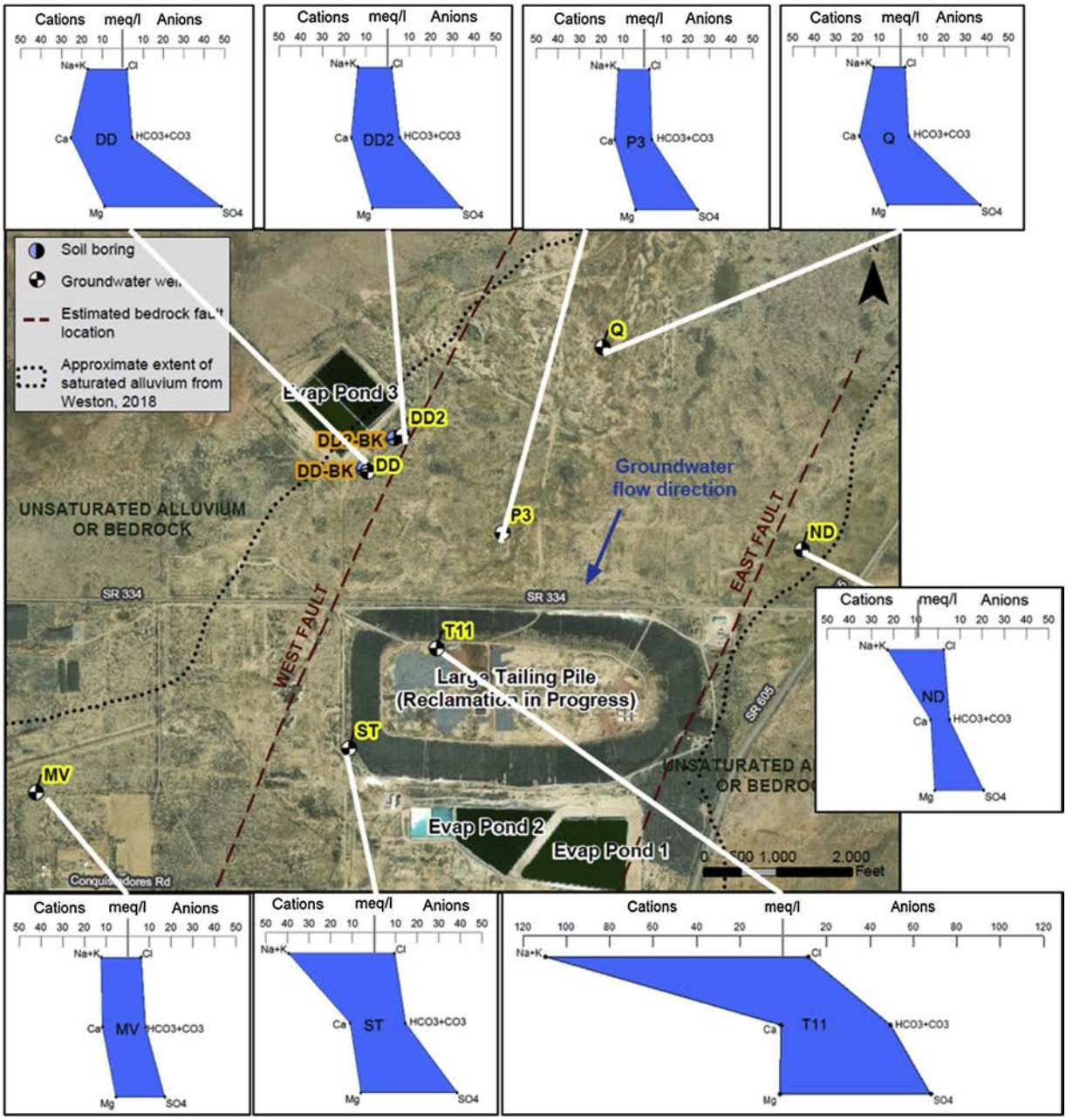

Fig. 7. Stiff diagrams indicate relative concentrations of major and minor cations and anions in groundwater. Wells upgradient to the site do not show characteristic signs of contamination, such as very high sodium (Na) and potassium (K). Ca – calcium, Cl – chloride, $HCO_3 + CO_3$ – bicarbonate and carbonate, meq/l – milliequivalents per liter, Mg – magnesium, SO_4 – sulfate.

molybdenum is not highly labile in alluvial groundwater at the site and that it is associated with seepage from the LTP (Hydro-Engineering, 2018). Molybdenum is measured at concentrations of 23.2 mg/L at well T11 and approximately 7 mg/L at well ST located on the southwest corner of the LTP. Molybdenum was also detected at a concentration of 0.02 mg/L at well MV, located in the site-affected area. Due to its association with LTP seepage, molybdenum can be used as a tracer of LTP-affected groundwater; geochemical modeling of waters at the GRP show that molybdenum is predicted to be present predominantly as soluble molybdate (MoO_4^{2-}) in tailing porewater and groundwater and to exhibit slightly more sorption to iron mineral phases than uranium (HMC, 2019). Molybdenum concentrations at upgradient wells DD and DD2 are an order of magnitude lower at 0.002 and 0.001 mg/L, respectively.

Selenium concentrations in the alluvial aquifer vary from 0.005 mg/L at upgradient well DD2 to 0.416 mg/L in upgradient well Q. At locations affected by LTP seepage, the selenium concentrations vary from 0.151 mg/L (well T11) to 0.033 mg/L (well MV). The

concentration at well DD (0.114 mg/L) is much higher than at well DD2 (0.0005 mg/L), even though they are close to each other (approximately 500 feet).

Isotopic analysis of sulfate and uranium was conducted to gain additional insight into the source of water and solutes in groundwater. Sulfate $\delta^{34}S$ values for site groundwater samples vary from -30.4 per mille (‰) to 7.7‰, and sulfate concentrations vary from 244 to 4670 mg/L (Supplemental S-3). Groundwater samples collected from the upgradient alluvial aquifer wells DD, DD2, P3, and Q exhibit $\delta^{34}S$ values varying from -30.4‰ to -25.5‰ and sulfate concentrations ranging from 931 to 2330 mg/L.

The uranium activity ratio (UAR), defined as the ratio of U-234 to U-238, was calculated to evaluate potential sources of uranium to groundwater. The UAR in rock material or in water resulting from acidic or alkaline milling generally has an isotopic ratio of 1 or very near 1 due to the similar leach rate for both isotopes during these processes (Zielinski et al., 1997). Natural weathering favors leaching of U-234, which is more unstable and is more prone to dissolve into groundwater compared to U-238 (Dosetto et al., 2008). Consequently, waters with a UAR much greater than 1 indicate a natural source. Water sampled from wells associated with the LTP (e.g., T11, ST, and MV in the downgradient affected area) exhibit a UAR of 1.2 or lower (generally close to 1). Groundwater from wells DD and DD2 exhibit a UAR of approximately 1.5, and other upgradient wells exhibit a UAR greater than 1.2 (Table 3; Supplemental S-4).

4. Discussion

Data from the 2016 groundwater sampling and geophysical assessment and 2018 core sampling and geophysical assessment indicate that the uranium in groundwater at locations upgradient of the LTP is present due to dissolution of natural uranium from native aquifer sediments. Lithology and alluvium composition suggest that uranium in alluvial sediments, which is concentrated in discrete layers, consists of eroded material from ore-rich formations to the north. Subsequent changes in redox chemistry, either at a macro- or micro-scale, has resulted in cycling of uranium between alluvial sediments (solid phase) and groundwater (dissolved phase), predominantly to/from lower-permeability sediments. These processes occur at interfaces between low- and high-permeability sediments, where groundwater flowing in higher permeability coarse-grained material interacts with less permeable domains through diffusion into and out of the silts and clays. The work completed by USGS at the GRP and at upgradient locations hypothesize that interbedded sands and clays at wells DD and DD2 may play a role in developing oxic and reduced water interfaces within the clay beds, resulting in mobilization of oxidized uranium from the sediments; they also suggest that collection and analysis of core samples, such as has been conducted in this study, could provide additional insight into this hypothesis (Harte et al., 2019).

4.1. Alluvium composition and lithology identify eroded ore-deposit layers

Alluvium in the lower Basin formed through deposition of eroded material from bedrock formations surrounding the GRP, which include the ore-bearing Morrison Fm. The abrupt transitions between lithology types observed in the boring logs support that sediment deposition occurred primarily through episodic fluvial deposition (ephemeral or meandering streams or flood events) versus sustained, large rivers which would lead to deposition of more gradually graded sediments. Clasts range from rounded to some angular grains, though the majority are sub-rounded, indicating that the sediments were transported a moderate distance from their source (Novak-Szabo et al., 2018). Microscopy and petrographic microscopy results show that the sediments reflect erosion products from upgradient ore-bearing formations. Potassium feldspar, which has only been reported in the Westwater Canyon and Brushy Basin Members and sparsely in the Dakota Sandstone, is encountered in samples at depths ranging from 9 to 72 feet bgs. The lack of potassium feldspar in other bedrock units in the area means that eroded material from the Westwater Canyon and Brushy Basin Members of the Morrison Fm. was a significant contributor to the formation of the alluvium in the lower Basin. The presence of trace volcanic glass (e.g., borehole DD2-BK at 25–26 feet bgs) reflects minimal erosion from the nearby Mount Taylor volcanic field.

Thorium-potassium ratios calculated from natural gamma ray spectroscopy analyses, using the method of Quirien et al. (1982), show that a majority of the clays in the samples are classified as mixed layer clays and montmorillonite, which is the primary clay associated with the Brushy Basin Member of the Morrison Fm. and Morrison Fm. in general (Santos, 1970; Brookins, 1982). Sediments on the eastern side of the alluvial channel (e.g. location ND, Fig. 8 points 41, 42, 43) have a generally lower thorium-potassium ratio and are considered less chemically weathered with illite and micas than sediments on the western side of the alluvial channel (e.g. locations DD, DD2) with mixed-layer clays, montmorillonite, chlorite and kaolinite, suggesting that the provenance of the sediments is different between the two areas (Fitzgerald et al., 2016). This is likely due to additional sedimentary inputs to the eastern side of the alluvial channel from the Lobo Creek Drainage (Fig. 1). The primary difference in the highland bedrock units between the two areas is the presence of recently deposited volcanics in the east (basalts and rhyolite of La Jara Mesa and the East Grants Ridge) and the apparent decreasing thickness of the Morrison Fm. units on the eastern side of the Basin, resulting in very little aerial exposure of the ore-bearing rock (Cather, 2011; Thaden et al., 1967). This difference in sediment origin and therefore host-rock deposition and weathering profile of the deposited materials is a possible explanation for why groundwater uranium concentrations at well ND on the eastern side of the alluvial channel are approximately an order of magnitude lower than those on the western side of the alluvial channel. Weathering of the sediments deposited on the western side of the channel across this section has been greater and the sediments have released uranium through the weathering process.

In addition to uranium detected in the saturated zone, uranium was found in samples collected from the vadose zone that are hydrologically isolated in the center of clay deposits. This indicates that the uranium could neither be present due to contact with uranium-bearing groundwater (the samples are approximately 30 feet above the water table) nor present due to contact with uranium-bearing infiltrating surface water (because the samples were collected from the middle of thick sequences of clay deposits,

Table 3
Groundwater Analytical Results for 8 Alluvial Groundwater Wells, Grants Reclamation Project.

Chemical Name	Fraction	Location Date Units	DD 10/6/2016	DD2 10/7/2016	MV 10/5/2016	ND 10/4/2016	P3 10/4/2016	Q 10/6/2016	ST 10/6/2016	T11 10/7/2016
Field Measurements										
Dissolved Oxygen		mg/l	3.37	NA	2.87	6.07	1.98	0.05 U	0.15	NA
Iron (Ferrous)	dissolved	mg/l	0.01 U	0.26	0.06	0.52	0.06	0.01 U	0.01 U	0.01 U
Eh (vs. SHE)		millivolts	256	253	258	256	243	252	306	260
pH		pH units	7.15	6.88	6.95	7.82	7.41	7.21	7.28	9.69
Specific Conductance at 25 degrees Celcius		mS/cm	4.057	3.165	2606	2.666	3.343	2.204	3.918	9.989
Temperature		deg C	13.6	13.1	14.3	13	12.9	13	14	14.9
Turbidity		ntu	2.66	0.61	0.58	1.98	0.37	0.34	1.05	3.15
Laboratory Analytical - Anions [EPA Method 300.0 except for nitrate/nitrite (EPA Method 353.2), ammonia (SM4500), alkalinity (EPA 2320B), and total organic carbon (SM5310C)]										
Alkalinity (as CaCO3)	total	mg/l	238	291	419	260	173	188	729	2140
Ammonia Nitrogen	total	mg/l	0.05 U	0.05 U	0.05 U	0.05 U	0.05 U	0.05 U	0.05 U	0.034 J
Bromide	total	mg/l	0.5	0.5	0.36 J	1.1	0.7	0.6	0.6	0.8 DJ
Chloride	total	mg/l	79	73	222	93	81	73	340 D	410 D
Fluoride	total	mg/l	0.5 D	0.2	0.3	0.8 D	0.5 D	0.3	0.6	5 D
Nitrate/Nitrite	total	mg/l	16 D	0.1 U	1.7 D	2.9 D	12 D	16 D	1.3	0.3
Sulfate	total	mg/l	2330 D	1650 D	826 D	988 D	1180 D	1770 D	1850 D	3270 D
Total Organic Carbon	total	mg/l	2.6	1.8	0.8	2.8	1.6	1.8	2.5	22.2 D
Laboratory Analytical - Major Cations and Metals/Metalloids (Cations (EPA Method 200.7) and trace elements (EPA Method 200.8)]										
Aluminum	dissolved	mg/l	0.0055 J	0.0086 J	0.0026 J	0.0032 J	0.0037 J	0.0022 J	0.0065 J	0.04
	total	mg/l	0.015 J	0.0063 J	0.0055 J	0.04	0.0053 J	0.0051 J	0.0045 J	0.1
Calcium	dissolved	mg/l	509	335	233	68.4	276	385	221	21
	total	mg/l	482	345	240	65.4	275	410	205	21.9
Iron	dissolved	mg/l	0.03 U	0.92	0.03 U	0.03 U	0.03 U	0.03 U	0.03 U	0.04
	total	mg/l	0.01 J	0.85	0.03 U	0.029 J	0.003 J	0.03 U	0.03 U	0.1 D
Magnesium	dissolved	mg/l	109	85.3	65.1	18.2	50.8	75.8	73.4	18.2
	total	mg/l	106	86.5	63	17.8	49.4	72.3	69.3	17.8
Molybdenum	dissolved	mg/l	0.002	0.001	0.02	0.005	0.001	0.002	6.8	23.2
	total	mg/l	0.001	0.001	0.021	0.005	0.002	0.002	7.58	23.4
Potassium	dissolved	mg/l	6.2	5.8	8.2	1.1	5.4	7.3	5.6	4.2 D
	total	mg/l	6.1	5.9	8.1	1.1	5.3	6.9	5.1	4.6 D
Selenium	dissolved	mg/l	0.114	0.0005 J	0.033	0.131	0.276	0.416	0.176	0.144 D
	total	mg/l	0.103 D	0.00057 J	0.031	0.115	0.254	0.38	0.153	0.151
Sodium	dissolved	mg/l	392	311	275	526	276	284	904 D	2520 D
	total	mg/l	388	320 D	271	511	264	273	850 D	2630 D
Vanadium	dissolved	mg/l	0.00025 J	0.00044 J	0.0018 J	0.008 J	0.01 U	0.00056 J	0.0023 J	0.09
	total	mg/l	0.01 U	0.01 U	0.002 J	0.0075 J	0.00043 J	0.00048 J	0.0027 J	0.09
Laboratory Analytical - Radionculides [Isotopic uranium by EPA Method 908.0)]										
Uranium	dissolved	mg/l	0.0944	0.218	0.249	0.0195	0.0201	0.0523	4.49	8.39
	total	mg/l	0.0869	0.221	0.242	0.0188	0.0209	0.0525	4.82	8.22
Uranium, Activity	dissolved	pCi/l	63.9	147	169	13.2	13.6	35.4	3040	5680
	total	pCi/l	58.8	150	164	12.8	14.1	35.6	3260	5570
Uranium-234	total	pCi/l	39.6	89.6	79.9	9.3	9.5	20.4	1700	2680
Uranium-235	total	pCi/l	1.3	3	3.3	0.3	0.6	0.7	75.7	120
Uranium-238	total	pCi/l	27.3	60.5	73.5	6.6	6.8	16.4	1660	2620
UAR	total	pCi/l	1.45	1.48	1.09	1.41	1.40	1.24	1.02	1.02

Notes: Total samples were unfiltered; Dissolved samples were filtered (0.45 μms).
Eh = oxidation-reducon potential.
SHE = standard hydrogen electrode.
NA = not analyzed.
mg/l = milligrams per liter.
pCi/l = picocuries per liter.
mS/cm = microSiemens per centimeter.
deg C = degrees Celscius.
ntu = nephelometric turbidity units.
UAR = uranium activity ratio.
Result Flags:
D = sample was diluted.
J = estimated value between method detection limit and reporting limit.
U = not detected above method detection limit; method detection limit shown.

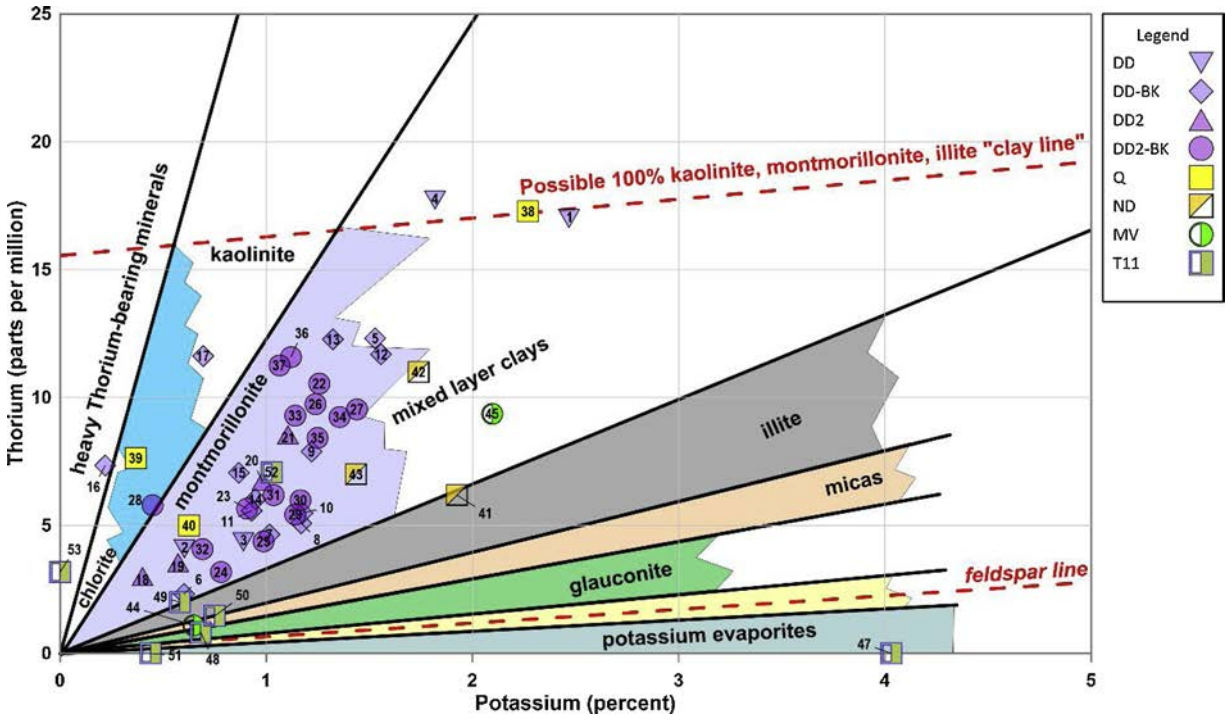

Fig. 8. Thorium-potassium cross-plot for mineral identification using spectral gamma ray spectroscopy data (modified from Glover, 2012) and soil results of wells DD, DD2, MV, ND, Q, and T11 and boreholes DD-BK and DD2-BK.

where penetration by percolating water would be limited and controlled by capillary forces). The highest soil uranium concentration of 10 mg/kg was encountered at borehole DD2-BK in the clay layer in the vadose zone at 11 to 12 feet bgs. Groundwater was encountered at 42 feet bgs, the shallowest it has been recorded at well DD or DD2. Given the shallow depth and its insulation from water contact, we can conclude that the uranium in this sample was emplaced during formation of the alluvium itself. This sample is rich in potassium feldspar and organic matter, as are common in the uranium-bearing Morrison Fm. units.

4.2. Uranium storage and release in the alluvial sediments

The most common features in sediments collected from the lower Basin in this study (mixed presence of oxidized/reduced minerals and predominance of organic-rich clays in contact with coarse-grained sediments that host oxic groundwater) indicate that redox conditions have varied over time, which can greatly affect uranium mobility and can contribute to heterogeneous distribution of natural uranium within sediments. Organic carbon is a persistent source of reducing power in the alluvial system, and iron oxides can sorb uranium. These microenvironments are important because they can concentration uranium in sediments. The majority of the samples contain metal sulfides, particularly notably as pyrite framboids. Pyrite framboids are most often formed by sulfate-reducing microbes (SRB) through the reduction of sulfate to sulfide (Qafoku et al., 2009). The framboids are made up of cubic and octahedral pyrite crystals that are roughly uniform in size and aggregate in a spherical structure. Over time, in an oxidizing environment, the pyrite can transform into iron oxides. This is seen in a SEM micrograph from borehole DD2-BK at 51–52 feet bgs, where most of the pyrite in two framboids has been converted to iron oxides, but select pockets of iron sulfide remain in the center of one of the framboids, where oxidizing agents presumably have not yet penetrated (Fig. 5F). This process is important for a number of reasons: 1) the formation of pyrite by SRB fractionates sulfur because the SRB preferentially use the lighter sulfur isotope (Krouse and Grinenko, 1991); 2) oxidation of pyrite originally formed by SRB dissolves the pyrite and releases isotopically light sulfate into groundwater (supported by the light sulfate measured in groundwater in the lower Basin, data presented below); 3) pyrite is known to be a scavenger of uranium (Stubbs et al., 2006; Qafoku et al., 2009), and the oxidation of pyrite as seen here could release entrained uranium to groundwater; and 4) the presence of pyrite signals that, at one time, the alluvial materials (whether saturated or unsaturated) were reducing, potentially driving uranium precipitation (Descostes et al., 2010). The transition of the alluvial system or microenvironments therein from reducing to oxidizing has the potential to release uranium through dissolution of pyrite, but also through oxidation of uranium (IV) to uranium (VI). As discussed previously, uranium (VI) is highly mobile, especially in water with high alkalinity. The presence of sulfide minerals and their oxidation products (e.g., sulfate) in the aquifer system near DD and DD2 provide evidence of a mechanism for sourcing uranium to groundwater from naturally occurring minerals. The results of the USGS analysis of uranium retrieved from multi-level PDS deployment show that the highest uranium concentrations in groundwater are within the depth horizon of finer-grained lithologic units, demonstrating that these processes (oxidation/dissolution) occur at contact

points between the oxidizing, carbonate-rich groundwater and uranium minerals that reside within these units (HMC, 2018; Harte et al., 2019). The USGS conclusions further support this by highlighting the poor relation between uranium and selenium at wells DD and DD2, indicating a non-anthropogenic source of uranium at these locations (Harte et al., 2019).

4.3. Stable sulfur isotopes as an indicator of the mechanism of sulfide mineral formation in the alluvial sediments

Sulfate δ^{34}S values in site-affected wells T11 and MV were -5‰ and 6.7‰, indicating contributions of heavy sulfur to the system, most likely from gypsum dissolution or sulfuric acid used during uranium ore milling. Sulfate δ^{34}S values for upgradient well groundwater samples are -30.4‰ at well Q, -26.2‰ at well DD, -28.7‰ at well DD2, and -4.9‰ at well ND. Jensen (1958) demonstrated that sulfur associated with uranium ores had δ^{34}S values ranging from -48‰ to 12‰; however, most values were strongly negative. Fishman and Reynolds (1982) reported δ^{34}S values ranging from -41.6‰ to -29.4‰ for pyrite associated with uranium ore samples collected from the Mariano Lake New Mexico uranium ore deposit. The δ^{34}S values less than -25‰ for these upgradient groundwater samples (excluding well ND) indicate that sulfate was derived from oxidation of a reduced sulfur form such as pyrite. Pyrite is seen via XRD and SEM-EDS in alluvial aquifer sediments, including hydraulically isolated clays, from boreholes DD-BK and DD2-BK. As discussed previously, framboidal pyrite is pervasive through most samples and is often associated with clay. Pyrite framboids are likely too friable to transport coherently and likely disintegrated due to physical and chemical destruction in oxic surface waters during transport; therefore, pyrite framboids must have formed in-situ. Because most framboids are formed by SRB, the pyrite must have formed relatively soon after initial deposition of sediments, where the sediment was protected enough from oxic flowing water to become reducing as recently deposited organic matter began to decay and SRB were able to drive sulfate reduction. As discussed, the subsequent oxidation of sulfide minerals represents a uranium release mechanism through mineral dissolution and direct oxidation of solid-phase uranium to dissolved-phase uranium.

4.4. Groundwater geochemistry

Groundwater analysis identified several distinguishing indicators of site-related contamination due to the LTP, including very high sodium and potassium concentrations, elevated molybdenum (> 0.005 mg/L), and UARs of less than ~ 1.2. Wells on site and in the affected area downgradient of the site (T11, ST, and MV) exhibit all three indicators of contamination, while wells upgradient of the site (DD, DD2, P3, Q, and ND) do not exhibit signs of contamination from the LTP. Wells DD and DD2, which are located near Evaporation Pond 3 (EP-3), do not exhibit signs of contamination by evaporation pond water such as very high sodium and potassium. No water has been detected in the Leak Detection and Collection System at EP-3 (Hydro-Engineering, 2018).

5. Conclusions

This study demonstrates that characterization of alluvial groundwater systems requires use of geologic, geophysical, mineralogical, and chemical methods to fully characterize the sources and background water quality conditions. Multidisciplinary methods are critical to validate and support established background groundwater concentration values to achieve regulatory closure of uranium mine and processing facilities. Sediment cores lithologically logged from boreholes DD-BK and DD2-BK indicate significant vertical heterogeneity including an alternating sequence of clays, silts, silty-sands, sandy-silts, sands with various amounts of gravel, and occasional gravel layers. Previous drilling logs based on lower-resolution sampling and visual soil descriptions suggested that the alluvium was uniform with very low variability in lithology; however, the alluvial sequence is much more heterogeneous than previous drilling logs have interpreted. Heterogeneity is also noted in the variable levels of gamma radiation measured at different lithological layers throughout each borehole. Discrete depth intervals with elevated radioactivity counts are indicated in alluvial sediments from both the saturated and unsaturated zones, from various lithological types of materials. Sedimentary materials in the alluvium contain radioactive constituents deposited differentially as part of the natural depositional sequence. Likewise, downhole geophysical logging indicates that the alluvium is laterally highly variable even over short distances. The fine-grained materials are found to correlate with elevated uranium from spectral gamma analysis, most closely in the lower two units.

Mineralogical analyses show that the alluvium at DD-BK and DD2-BK was derived from source rock containing unaltered feldspars, claystones that include kaolinite, and arkosic sandstones like those found at the upgradient northern boundary of the basin in the Westwater Canyon and Brushy Basin Members of the Morrison Fm. Local bedrock is likely the source of uranium deposited into sediments by fluvial transport and dissolution/reprecipitation in the alluvium. These alluvial sediments have undergone weathering to variable extents as indicated by the thorium-potassium relationship in sediments distributed across the alluvial valley, leaching uranium to groundwater at variable concentrations, with higher concentrations associated with fine-grained sediment. Consistent with this model, geochemical analyses indicate that, in general, uranium and vanadium co-occur at higher concentrations. For example, soil recovered from DD-BK exhibits higher vanadium concentrations when uranium is detectable. The highest uranium concentration was encountered in the unsaturated zone, indicating that uranium in alluvial deposits is naturally derived due to transport and deposition of naturally uranium-rich materials over hundreds to thousands of years.

A significant aspect of the occurrence of uranium in groundwater from natural sources is the dynamic nature of uranium relative to redox interfaces and cycling between soluble and immobile uranium forms. Evidence of redox interfaces, active to present day, is provided in the sediment mineralogy; the detection of framboidal pyrite that has been partially converted to iron oxides indicates that a redox change has occurred but that some reduced minerals remain. What was once a strongly reducing environment, supporting the formation and presence of pyrite, is now undergoing oxidation. The presence of sulfate minerals in DD-BK and DD2-BK, including

large crystals of gypsum, also supports this transition to an oxidized system. Such a change can result in the release of uranium due to oxidation of low-solubility uranium (IV) to high-solubility/high-mobility uranium (VI). This is a source of leaching of uranium from solid alluvial materials to groundwater.

This work suggests that the material in which the well is screened may affect the chemistry of water in the well. Wells screened in coarse-grained sediments may preferentially sample groundwater with geochemistry that is dominated by relatively fast-flowing regional groundwater. Wells screened in fine-grained sediments may preferentially yield samples of groundwater with geochemistry that has been influenced by the presence of a greater source term (higher concentration of uranium in fines) and lower hydraulic conductivity that prevents dilution or washout of constituents. Shorter screens across targeted lithologic units may provide greater resolution of ambient uranium concentrations and potential spatial variability in concentrations. A comprehensive hydrogeological characterization and monitoring approach is particularly important in groundwater systems in areas known to harbor mineralization of economic viability, such as the Grants Mineral Belt, where the natural occurrence of uranium minerals in alluvial sediments leads to a heterogeneous distribution of uranium concentrations in groundwater. The concentrations of uranium in groundwater in this system are greater than the Federal water quality standards; as such, site-specific standards have been established and are supported by the findings of this work, including: 1) the detection of the occurrence of uranium in unsaturated and saturated zone alluvial sediments, 2) groundwater chemical composition conducive to the mobilization of uranium out of the sediments, 3) the presence of weathered and unweathered pyrite minerals demonstrating a uranium-mineral host phase (along with organic matter), and 4) results of leaching of the alluvial sediments showing uranium mobilization from the sediments and evolution of uranium concentrations in the leachate to concentrations approximating that observed in the groundwater. Alluvial groundwater systems derived from weathered mineralized bedrock therefore require careful evaluation of water quality to understand background conditions; in this case, uranium in groundwater results from the influence of chemical dissolution processes occurring at the interface of fine and coarse grained sediments within the aquifer.

The field work (drilling, sample collection, and geophysics) and laboratory analyses and reporting associated with this manuscript was funded by Homestake Mining Company of California, a subsidiary of Barrick Gold Corporation. The authors certify that the funding source had no bearing on the interpretation of the data and associated conclusions presented in the manuscript.

Declaration of Competing Interest

The field work (drilling, sample collection, and geophysics) and laboratory analyses and reporting associated with this manuscript was funded by Homestake Mining Company of California, a subsidiary of Barrick Gold Corporation. The authors certify that the funding source had no bearing on the interpretation of the data and associated conclusions presented in the manuscript.

Acknowledgements

The authors would like to thank Ron Schott at DCM Science Laboratories in Wheat Ridge, Colorado for expert mineralogy assistance and numerous discussions of standard and innovative mineral and element identification methods.

Appendix A. Supplementary data

Supplementary material related to this article can be found, in the online version, at doi:https://doi.org/10.1016/j.ejrh.2019.100636.

References

Beath, O.A., Gilbert, C.S., Eppson, H.F., 1940. The use of indicator plants in locating seleniferous areas in Western United States. III. Further Studies. Botany 27 (7), 564–573.

Blake, J.M., De Vore, C.L., Avasarala, S., Ali, A.-M., Roldan, C., Bowers, F., Spilde, M.N., Artyushkova, K., Kirk, M.F., Peterson, E., Rodriguez-Freire, L., Cerrato, J.M., 2017. Uranium mobility and accumulation along the Rio Paguate, Jackpile Mine in Laguna pueblo. NM. Environ. Sci.-Proc. Imp. 19, 605–621.

Blake, J.M., Harte, P., Becher, K., 2019. Differentiating anthropogenic and natural sources of uranium by geochemical fingerprinting of groundwater at the Homestake uranium mill, Milan, New Mexico, USA. Environ. Earth Sci. 78 (384).

Brookins, D.G., 1979. Uranium Deposits of the Grants, New Mexico Mineral Belt. Grand Junction: U.S. Department of Energy Report DOE/BFEC 76-029E.

Brookins, D.G., 1982. Geochemistry of clay minerals for uranium exploration in the Grants mineral belt, New Mexico. Miner. Deposita. 17, 37–53.

Brookins, D.G., 1990. Clay minerals in sandstone uranium deposits: radwaste applications. In: Proceedings of the 9th International Clay Conference, Strasbourg, 1989. Vol III: Geochemistry of Clays. Nuclear waste disposal. Strasbourg: Institut de Géologie – Université Louis-Pasteur, 1990. pp. 85–96 (Sciences Géologiques. Mémoire, 87).

Cannon, H.L., 1953. Geobotanical Reconnaissance Near Grants, New Mexico. United States Geological Survey Circular, Washington, D.C, pp. 264.

Cather, S., 2011. Preliminary Geologic Map of the Dos Lomas Quadrangle, Cibola and McKinley Counties, New Mexico. New Mexico Bureau of Geology and Mineral Resources Open-file Digital Geologic Map OF-GM 219.

Chenoweth, W.L., Holen, H.K., 1980. Exploration in Grants uranium region since 1963. In: Rautman, C.A. (Ed.), Geology and Mineral Technology of the Grants Uranium Region 1979. New Mexico Institute in Mining and Technology Symposium Proceedings May 13-16, 1979.

Descostes, M., Schlegel, M.L., Eglizaud, N., Descamps, F., Miserque, F., Simoni, E., 2010. Uptake of uranium and trace elements in pyrite (FeS_2) suspensions. Geochim. Cosmochim. Ac. 74 (5), 1551–1562. https://doi.org/10.1016/j.gca.2009.12.004. Elsevier Ltd.

Dodge, C.J., Francis, A.J., Gillow, J.B., Halada, G.P., Eng, C., Clayton, C.R., 2002. Association of uranium with iron oxides typically formed on corroding steel surfaces. Envir. Sci. Tech. 36, 3504–3511.

Dosetto, A., Bourdon, B., Turner, S.P., 2008. Uranium-series isotopes in river materials: insights into the timescales of erosion and sediment transport. Earth Planet Sc. Lett. 265, 1–17.

Ellis, D.V., Singer, J.M., 2008. Well Logging for Earth Scientists, 2nd edition. Springer, P.O. Box 17, 3300 AA Dordrecht, The Netherlands.

Finch, R., Murakami, T., 1999. Systematics and paragenesis of uranium minerals. In: Burns, P.C., Finch, R. (Eds.), Uranium: Mineralogy and Geochemistry and the Environment, Rev. Mineral. Volume 38, 679 pp.
Fishman, N., Reynolds, R., 1982. Origin of the Mariano Lake uranium deposit, McKinley County, New Mexico. United States Geological Survey Open-File Report 82-888.
Fitzgerald, D., Nadon, G., Thomas, B., 2016. Clay mineralogy, provenance, and sequence stratigraphy of Upper ordovician shales in Eastern Ohio. In: Adapted from Oral Presentation Given at AAPG 2016 Eastern Section Meeting. Lexington, Kentucky, September 25–27, 2016.
Freeman, V.L., Hilpert, L.S., 1956. Stratigraphy of the morrison formation in part of northwestern New Mexico. Contributions to the geology of uranium. United States Geological Survey Bulletin 1030-J. 309-334.
Gallaher, B.M., Cary, S.J., 1986. Impacts of Uranium Mining on Surface and Shallow Ground Waters, Grants Mineral Belt, New Mexico. New Mexico Environmental Improvement Division, Santa Fe, NM Report EID/GWH-86/2.
Glover, P.W.J., 2012. Petrophysics MSc. Course Notes. University of Nottingham, UK.
Granger, H.C., 1963. Mineralogy. In: Kelley, V.C., The Society of Economic Geologists (Eds.), Geology and Technology of the Grants Uranium Region, Memoir 15. State Bureau of Mines and Mineral Resources, New Mexico Institute of Mining and Technology, pp. 21–37.
Granger, H.C., Warren, C.G., 1974. Zoning in the altered tongue associated with roll-type uranium deposits. In: Formation of Uranium Ore Deposits, Proceedings of a Symposium Athens. International Atomic Energy Agency, May 6–10.
Harte, P.T., Blake Becher, J.M.K.D., 2018. Determination of representative uranium and selenium concentrations from groundwater, 2016, Homestake Mining Company Superfund site. USGS Open File Report 2018-1055, Milan, New Mexico.
Harte, P.T., Blake, J.M., Thomas, J., Becher, K., 2019. Identifying natural and anthropogenic variability of uranium at the well scale, homestake superfund site, near Milan, New Mexico, usa. Environ. Earth Sci. 78–95. https://doi.org/10.1007/s12665-019-8049-y.
Heinrich, E.W., 1958. Mineralogy and Geology of Radioactive Raw Materials. McGraw-Hill Book Co., Inc., New York 654pp.
Hilpert, L.S., 1969. Uranium Resources of Northwestern New Mexico. US Atomic Energy Commission, Geological Survey Professional Paper 603. 166 p.. .
Homestake Mining Company (HMC), 2012. Grants Reclamation Project Updated Corrective Action Program (CAP). Homestake Mining Company of California March 2012.
HMC, 2018. Evaluation of Water Quality in Regard to Site Background Standards at the Grants Reclamation Project. Homestake Mining Company of California, Grants Reclamation Project. September 2018. NRC ADAMS Accession Number ML19025A300. https://adamswebsearch2.nrc.gov/webSearch2/main.jsp?AccessionNumber=ML19025A300.
HMC, 2019. Preliminary Groundwater Flow and Transport Model Status Report. Homestake Mining Company of California Grants Reclamation Project. March 2019.
Hydro-Engineering, 2018. 2017 Annual Monitoring Report/Performance Review for Homestake's Grants Project Pursuant to NRC License SUA-1471 and Discharge Plan DP-200. March 2018. NRC ADAMS Accession No. ML18102A955. .
Jensen, M., 1958. Sulfur isotopes and the origin of sandstone-type uranium deposits [Colorado Plateau and Wyoming]. Econ. Geol. 53 (5), 598–616.
Johnson, R.H., Tigar, A., Morris, S., Campbell, S., Tafoya, K., Bush, R., Frazier, W., 2018. Column tests and multilevel Well geochemistry to explain contaminant plume persistence issues downgradient of a former uranium mill site. In: Wolkersdorfer, Ch, Sartz, L., Weber, A., Burgess, J., Tremblay, G. (Eds.), 11th ICARD/IMWA/MWD Conference 2018: Risk to Opportunity. 10-14 September 2018, Pretoria, South Africa. International Mine Water Association. 9781510873285, .
Kohler, M., Curtis, G.P., Meece, D.E., Davis, J.A., 2004. Methods for estimating adsorbed uranium(VI) and distribution coefficients of contaminated sediments. Envir. Sci. Tech. 38 (1), 240–247. https://doi.org/10.1021/es0341236.
Krouse, H.R., Grinenko, V.A., 1991. Stable Isotopes: Natural and Anthropogenic Sulphur in the Environment. SCOPE 43. John Wiley & Sons, New York.
Langmuir, D., 1978. Uranium solution-mineral equilibria at low temperatures with applications to sedimentary ore deposits. Geochim. Cosmochim. Ac. 42 (6A), 547–569.
Lee, M.J., 1976. Geochemistry of the Sedimentary Uranium Deposits of the Grants Mineral Belt, Southern San Juan Basin, New Mexico. Ph.D. Dissertation. University of New Mexico 24 pp.
Lefebvre, P., Noël, V., Lau, K.V., Jemison, N.E., Weaver, K., Williams, K.H., Bargar, J.R., Maher, K., 2019. Isotopic fingerprint of uranium accumulation and redox cycling in floodplains of the Upper Colorado River Basin. Envir. Sci. Tech. https://doi.org/10.1021/acs.est.8b05593. In press.
Leopold, L.B., Snyder, C.T., 1951. Alluvial Fills Near Gallup, New Mexico. Contributions to Hydrology, 1948-51. United States Geologic Survey Water-Supply Paper 1110-A.
Liu, C., Shi, Z., Zachara, J.M., 2009. Kinetics of uranium(VI) desorption from contaminated sediments: effect of geochemical conditions and model evaluation. Envir. Sci. Tech. 43, 6560–6566.
Lovering, G.T., 1956. Radioactive deposits in New Mexico. U.S. Geological Survey, Bull. I009L. pp. 315–390.
Mast, M.A., Mills, T.J., Paschke, S.S., Keith, G., Linard, J.I., 2014. Mobilization of selenium from the Mancos Shale and associated soils in the lower Uncompahgre River Basin. Colorado. Appl. Geochem. 48, 16–27.
Maxwell, C.H., 1982. Mesozoic stratigraphy of the laguna-Grants region. In: Country IIAlbuquerque, Wells, S.G., Grambling, J.A., Callender, J.F. (Eds.), New Mexico Geological Society 33rd Annual Fall Field Conference Guidebook, pp. 261–265.
McLemore, V., 2007. Uranium resources in New Mexico. In: Proceedings of the Society of Mining, Metallurgy and Exploration Annual Meeting. Denver, CO.
McLemore, V.T., 2010. The grants uranium district, New Mexico: update on source, deposition, and exploration. The Mountain Geologist 48 (1), 23–44.
Meunier, J.D., 1994. The composition and origin of vanadium-rich clay minerals in Colorado Plateau Jurassic Sandstones. Clay Clay Miner. 42, 391–401.
New Mexico Administrative Code. Title 20, Chapter 6, Part 4. https://www.env.nm.gov/wp-content/uploads/2017/06/20.6.4-NMAC-Section-804-Integrated-Rule-20180228.pdf.
Novak-Szabo, T., Sipos, A.A., Shaw, S., Bertoni, D., Pozzebon, A., Grottoli, E., Sarti, G., Ciavola, P., Domokos, G., Jerolmack, D.J., 2018. Universal characteristics of particle shape evolution by bed-load chipping. Sci. Adv. 4, 1–11.
NRC. 2006. Homestake Mining Company – Grants, New Mexico – License Amendment No. 39 to Materials License No. SUA-1471 (TAC LU0122). Nuclear Regulatory Commission, NRC ADAM Accession No. ML061710354.
Pierson, C.T., Green, M.W., 1977. Factors controlling localization of uranium deposits in the Dakota Sandstone, Gallup and Ambrosia Lake Mining Districts, McKinley County, New Mexico. U.S. Department of the Interior Geological Survey Open-file Report 77-766, 62 pp.
Plant, J.A., Simpson, P.R., Smith, B., Windley, B.F., 1999. Uranium ore deposits – products of the radioactive earth. In: Burns, P.C., Finch, R. (Eds.), Uranium: Mineralogy, Geochemistry and the Environment. Mineralogical Society of America, Washington, D.C, pp. 255–319.
Qafoku, N.P., Kukkadapu, R., Mckinley, J.P., Arey, B.W., Kelly, S.D., Wang, C., Resch, C.T., Long, P.E., 2009. Uranium in framboidal pyrite from a naturally bioreduced alluvial sediment. Envir. Sci. Tech. 43 (22), 8528–8534.
Quirien, J.A., Gardner, J.S., Watson, J.T., 1982. Combined Natural Gamma Ray Spectral/Litho-Density Measurements Applied to Complex Lithologies: Society of PetRoleum Engineers Annual Meeting.
Santos, E.S., 1970. Stratigraphy of the Morrison Formation and Structure of the Ambrosia Lake District, New Mexico. Contributions to Economic Geology. United States Geological Survey Bulletin 1272-E. E1-E30.
Sherman, H.M., Gierke, J.S., Anderson, C.P., 2007. Controls on spatial variability of uranium in sandstone aquifers. Groundwater Mon. Rem. 27 (2), 106–118.
Smedley, P.L., Kinniburgh, D.G., 2017. Molybdenum in natural waters: a review of occurrence, distributions and controls. Appl. Geochem. 84, 387–432.
Spirakis, C.S., 1996. The roles of organic matter in the formation of uranium deposits in sedimentary rocks. Ore Geol. Rev. 11 (1–3), 53–69. https://doi.org/10.1016/0169-1368(95)00015-1.
Stewart, B.D., Mayes, M.A., Fendorf, S., 2010. Impact of uranyl-calcium-carbonato complexes on uranium adsorption to synthetic and natural sediments. Envir. Sci. Tech. 44 (3), 928–934.
Stubbs, J., Elbert, D.C., Veblen, D.R., Zhu, C., 2006. Electron Microbeam Investigation of Uranium-Contaminated Soils from Oak Ridge, TN, USA. Environ. Sci. Tech. 40 (7), 2108–2113.
Telfeyan, K., Johannesson, H., Mhajerin, T.J., Palmore, C.D., 2015. Vanadium geochemistry along groundwater flow paths in contrasting aquifers of the United States:

carrizo Sand (Texas) and Oasis Valley (Nevada) aquifers. Chem. Geol. 410, 63–78.
Thaden, R.E., Santos, E.S., Ostling, E.J., 1967. Geologic Map of the Dos Lomas Quadrangle, Valencia and McKinley Counties, New Mexico. United States Geologic Survey.
U.S. Department of Energy (USDOE), 2014. Site Status Report: Groundwater Flow and Contaminant Transport in the Vicinity of the Bluewater, New Mexico, Disposal Site. United States Department of Energy, Legacy Management Report LMS/BLU/S11381.
U.S. Code of Federal Regulations. Title 40, Part 141: National Primary Drinking Water Regulations https://www.epa.gov/sites/production/files/2019-03/documents/cfr-2011-title40-vol23-part141.pdf.
U.S. Geological Survey (USGS), 2016a. Field Investigations to Help Support the Assessment of Background Concentrations for Uranium (U) at the Homestake Mining Company, Superfund Site.
USGS, 2016b. Quality Assurance Project Plan. Field Investigations to Help Support the Assessment of Background Concentrations for Uranium (U) at the Homestake Mining Company, Superfund Site Near Milan, New Mexico. Prepared for the United States Environmental Protection Agency Superfund Division Region 6. Unsigned. July 26.
Vroblesky, D.A., Petkewich, M.D., Campbell, T.R., 2002. Field Tests of Diffusion Samplers for Inorganic Constituents in Wells and at a Ground-Water-Discharge Zone. USGS Water Resources Investigation Report 02-4031. Air Force Center for Environmental Excellence and the Southern Division Naval Facilities Engineering Command.
Vroblesky, D.A., Joshi, M., Morrell, J., Peterson, J.E., 2003. Evaluation of Passive Diffusion Bag Samplers, Dialysis Samplers, and Nylon-Screen Samplers in Selected Wells at Andersen Air Force Base, Guam, March–April 2002. USGS Water-Resources Investigations Report 03-4157. Air Force Center for Environmental Excellence.
Wright, M.T., Stollenwerk, K.G., Belitz, K., 2014. Assessing the solubility controls on vanadium in groundwater, northeastern San Joaquin Valley, CA. Appl. Geochem. 48, 41–52.
Wu, Y., Wang, Y., Guo, W., 2019. Behavior and fate of geogenic uranium in a shallow groundwater system. J. Contam. Hydrol. 222, 41–55.
Yoshida, H., Yui, M., Shibutani, T., 1994. Flow-path structure in relation to nuclide migration in sedimentary rocks. J. Nucl. Sci. Tech. 31 (8), 803–812.
Zielinski, R.A., Chafin, D.T., Banta, E.R., Szabo, B.J., 1997. Use of 234U and 238U isotopes to evaluate contamination of near-surface groundwater with uranium-mill effluent: a case study in south-central Colorado. USA. Environ. Geol. 32 (2), 124–136.